Hindawi
Advances in Civil Engineering
Volume 2022, Article ID 9228569, 23 pages
https://doi.org/10.1155/2022/9228569

Research Article

Study on Catastrophe Information Characteristics of Water Inrush in Karst Tunnel by Drilling and Blasting Method

Jiaqi Guo,[1] **Erbo Wang**,[1] **Yongbiao Lai**,[2] **Zhenyu He**,[3] **and Fan Chen**[1]

[1]*School of Civil Engineering, Henan Polytechnic University, Jiaozuo 454003, China*
[2]*China Construction Railway Investment Construction Group Ltd, Beijing 102601, China*
[3]*Henan Geological Engineering Survey Institute Co., Ltd., Zhengzhou 450001, Henan, China*

Correspondence should be addressed to Yongbiao Lai; 48084108@qq.com

Received 7 August 2022; Accepted 13 September 2022; Published 23 November 2022

Academic Editor: Xiaobo Zhang

When building tunnels in karst areas, the hidden high-pressure water-bearing karst caves are prone to cause geological disasters such as water inrush and mud gushing. In order to study the disaster process of water and mud resistant rock mass with the quasi-masonry structure and the accompanying catastrophe information of water inrush in karst tunnels by the drilling and blasting method, a new method based on the DEM and fictitious joint technology is adopted to simulate the evolution process of water inrush and study the evolutionary characteristics of catastrophe information like seepage pressure and displacement under the conditions of different joint inclination angles, tunnel depths, and thickness of the water and mud resistant rock mass. The research results show that (1) the seepage pressure and displacement in the water and mud resistant rock mass decrease and increase respectively along the water and mud resistant rock mass from top to bottom in the process of water inrush. (2) The displacement and seepage pressure in the water and mud-resistant rock mass increases with the increase of the joint inclination angle. The greater the tunnel depth and thickness of the water and mud-resistant rock mass, the faster the propagation speed of the fissure zone. (3) With the increase of the water and mud-resistant rock mass thickness, the failure mode of the tunnel outburst layer structure gradually changes from the overall collapse to the partial collapse of the vault to form a relatively stable slump arch. The research results can provide some guidance for tunnel construction in the karst tunnel.

1. Introduction

Karst geomorphology accounts for about 15% of the global area and is one of the most frequent adverse geological in the construction of underground transportation, water conservancy tunnels, and mine roadways and it is also a thorny problem faced by the world's engineers [1, 2]. As an important part of the traffic road network, tunnel projects often encounter various karst geological disasters during the construction of karst areas due to complex engineering geology and hydrogeology, development of karst disaster-causing structures, and active groundwater. The water inrush is one of the most common and extremely destructive geological disasters [3, 4]. Hundreds of water inrush accidents have occurred in China during the past few years, which have caused serious economic loss, engineer casualties, and environmental disruption [5–11] (see Figure 1). During the construction of the Maluqing tunnel of the Yichang-Wanzhou railway, 19 serious water and mud inrush disasters occurred one after another, and the instantaneous water inrush reached the highest level of railway construction in the world. Only two extraordinarily serious disasters occurred on January 21, 2006, and April 11, 2008, resulting in 15 deaths [12]. During the construction of the Yesanguan Tunnel, there was a sudden influx of water and mud, and the water inflow was about $5 \times 10^4\ m^3/h$. The disaster-caused 52 constructors to be trapped, many pieces of equipment washed, and 10 people dead [12]. When the construction mileage of the Telmo Tunnel for the Chengdu-Kunming railway capacity expansion and reconstruction project reached DK274 + 580, several water inrush disasters occurred on the tunnel face, which caused project shutdown

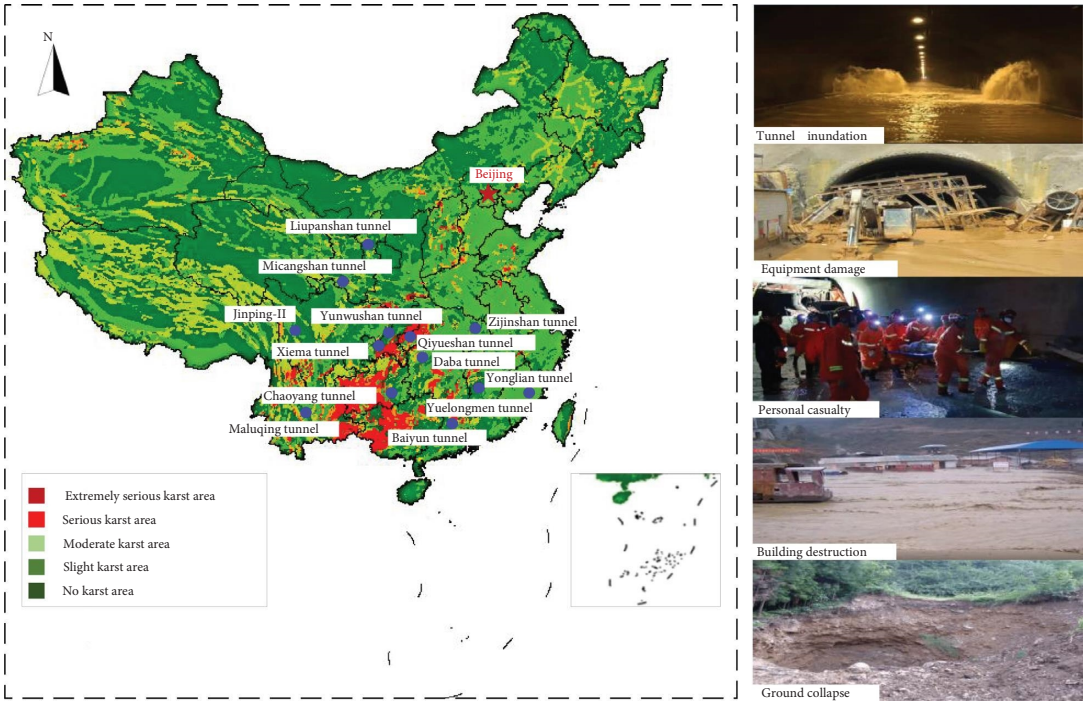

Figure 1: The typical water inrush accidents of karst tunnels and their effects in China.

and delay [13]. The main reason for the above disasters is that the research on the water inrush mechanism in karst tunnels drops behind the development of production practice. Therefore, it is of great significance to carry out relevant research about the evolution process and catastrophe evolution information characteristics of water inrush for prevention and control of water inrush in karst tunnel.

Water inrush in karst tunnels is a destabilizing process of outburst-proof rock mass under the coupled influence of multiple factors and is conditions and triggered by excavation disturbance. At present, many scholars have done a lot of research on the mechanism and the information characteristics of water inrush through theoretical analysis, model tests, and numerical simulation. In the field of theoretical analysis, Li et al. [14] deduced the critical water pressure of cracks that occurred through compression shear expansion failure under the action of explosion stress waves. Xu et al. [15] used slice synthetic and elastic mechanics theory to analyze the mechanical properties of filled karst caves located at the top, bottom, and sides of the tunnel and deduced the minimum safe thickness formula of water and mud resistant rock mass. Fu et al. [16] deduced the formula for calculating the minimum safe thickness of the karst cave below the excavation tunnel. Guo et al. [17] used a theoretical analysis method to study the stability of the outburst prevention rock mass between the tunnel and the latent cavity. The above instability criterion based on theoretical analysis can only be used to judge the rock stability in the final stage of the water inrush of karst tunnels. The water inrush in a tunnel involves crack initiation, expansion, and penetration, which is a highly nonlinear problem in mathematics. The model test can accurately simulate the rupture and instability processes of the outburst-preventing rock mass and truly reproduce the evolution process of water inrush. In the field of the model test, Li et al. [18] conducted a model test to discuss the influence of in-situ stress, water pressure, and the thickness of water and mud-resistant rock mass on the water inrush in karst tunnels. Kirsch [19] and Idinger et al. [20] studied the stability of tunnel faces through physical model tests. Huang et al. [21] carried out a model test to study the influence of excavation disturbance and aquifer thickness on the seepage failure of the intact water and mud-resistant rock mass. Due to the limitation of measuring elements number and their function, it is impossible to obtain enough macro information about the water inrush and it is also unable to grasp the meson information such as crack initiation, crack propagation, and the complex interaction process between water and rock. While the numerical simulation method could solve the above problems, and it has the function of visualizing the rupture process of outburst-proof rock.

At present, many scholars have used the numerical simulation method to study water inrush. Liu et al. [22] used the finite difference numerical calculation program to analyze the evolution law of the plastic zone, displacement field, and seepage field of the rock mass when the tunnel excavation approached the upper and lower lateral karst pipes. Zhao et al. [23] used the finite element numerical calculation method to study the influence of cavity sizes and the distances between the cavity at the top and the tunnel on the stability of surrounding rock. Qin et al. [24] used FLAC3D to analyze the distribution of releasable elastic strain energy and failure zone under different hidden cave widths. Lei [25] used a three-dimensional finite difference

program to simulate and analyze the influence of a water-filled hidden cave at the top on the stability of surrounding rock and established a mathematical model for predicting the minimum safe thickness between the cave and the tunnel through multiple regression analysis. Most of the above numerical simulations regard the outburst-proof rock as a porous continuous medium and do not consider the impact of tunnel blasting excavation. It also cannot simulate the formation, expansion, and penetration process of the seepage channel and the collapse process of surrounding rock. The discrete element method has obvious advantages in simulating the fracture process of rock mass, and it has been widely used in the field of civil engineering.

In view of this, this paper uses a new method based on the DEM considering the structural characteristics of water and mud resistant rock mass and explosive load in drilling and blasting method. This method is employed to simulate the process of water inrush in karst tunnel and reveals the influence law of joint dip angle, tunnel depth, and the thickness of water and mud resistant rock mass on the catastrophe characteristics of water inrush in karst tunnel. Moreover, the evolution characteristics of catastrophe information, including water pressure and displacement, were analyzed. The research results had great significance for early warning and prevention of water inrush in karst tunnel.

2. The Fluid-Structure Interaction Theory and Calculation Model Based on DEM

2.1. Numerical Solution Method

2.1.1. Motion Equation of Deformed Block. In the discrete element, the rock mass is divided into multiple deformable blocks by joints, and the deformable block is discretized into multiple constant-strain triangular elements by the grid, and the movement and deformation of the entire rock mass are reflected by the movement of the cell points [26].

(1) The equation of motion at cell point i:

$$\mu_i = \frac{\sum f_i + f_p + f_b}{m} + g_i, \tag{1}$$

$$f_i = f_i^c + \sum_{l=1}^{M}\left[\sigma_{ij}\sum_{k=1}^{N}\left(n_j^k \Delta s^k\right)\right]_l,$$
$$f_b = 2\left(\rho C_p\right)v_n, \tag{2}$$
$$C_p = \sqrt{\frac{K + 4G/3}{\rho}},$$

where μ_i is the displacement of the cell point; m is the concentrated mass assigned to the cell point; g_i is the acceleration of gravity; M is the number of elements connected to node I; N is the number of element nodes; n_j^k is the unit normal vector of the k-th edge in the element; Δl^k is the length of the k-th edge in the element; d is the thickness of the element; Δs^k is the element area; σ_{ij} is the element stress; f_i^c is the contact force between the blocks. f_p is the water pressure; f_b is the blasting load; ρ is the medium density; v_n is the longitudinal wave velocity; C_p is the normal velocity of the input particle; K is bulk modulus; and G is the shear modulus.

2.1.2. Laws of Fluid Motion. Assuming that the joints and fissures are smooth walls, the fluid flow in the joints and fissures follows Darcy's law [27]:

$$q_i = -k\left(p - \rho_f x_f g_i\right), \tag{3}$$

where k is the rock mobility coefficient; ρ_f is the fluid density; g_i is the components of the gravity vector.

2.1.3. Simulation Principle of Fracture Seepage

(1) Influence of Stress Field on Seepage Field. Discrete element numerical analysis can analyze the flow of fluid in the fissures of the impermeable block system. It is assumed that in the process of fluid flowing in the fissures, the rock mass is an impermeable material, and the fluid affects the displacement of the rock mass and changes the normal displacement of the block, thereby affecting the joint width affects the permeability of the jointed rock mass, namely [27]:

$$\mathrm{a} = a_0 + \mu_n. \tag{4}$$

(2) Influence of Seepage Field on Stress Field. The change of the pressure of the fluid in the joint on the joint wall causes the change in the stress state of the rock mass, and finally affects the deformation of the fractured rock mass. The osmotic pressure increase caused by the confluence of the fluid at a point is [27]:

$$\Delta \mathrm{q} = \frac{k_w}{V}\left(Q\Delta t - \Delta V\right), \tag{5}$$

where k_w is the bulk modulus of the fluid; Q is the total flow of the fluid entering the node; ΔV is the volume change. After deformation, the fluid penetration pressure and penetration force (see Figure 2) are as follows:

$$\mathrm{p} = p_0 + k_w Q\frac{\Delta t}{V} - k_w\frac{\Delta V}{V_m}, \tag{6}$$

$$F_i = \mathrm{p}n_i L, \tag{7}$$

where F_i is the seepage force of the joint and fissure; L is the length of the joint and fissure; and V_m is the mean volume. Substitute formula (7) into the f_i in formula (2), the displacement of the grid point under the influence of seepage pressure can be calculated, and the effect of the seepage pressure on the stress can be calculated.

2.2. Computation Model of Discrete Element Numerical

2.2.1. Water and Mud Resistant Rock Mass with the Quasi-Masonry Structure. The karst geological conditions are extremely complex. However, most of the existing numerical simulations assume that the karst strata are continuous homogeneous materials, and the influence of blasting,

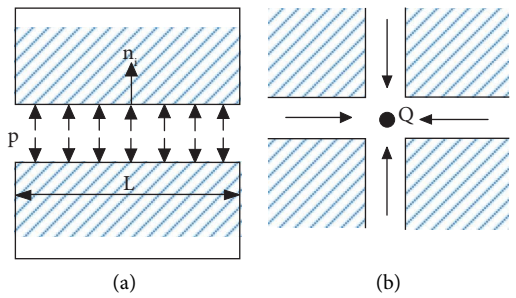

Figure 2: Effect of seepage pressure on stress field. (a) The effect of fluid on the block. (b) Increase in block seepage pressure.

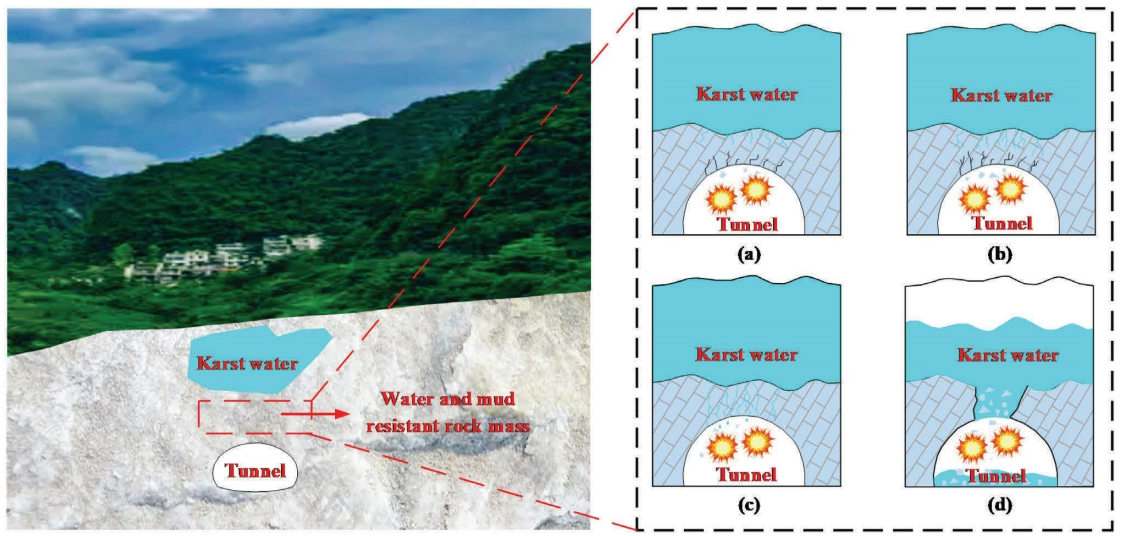

Figure 3: Sketch of the quasi-masonry structure of water and mud-resistant rock mass and water inrush process. (a) Crack initiation is induced by blasting excavation and hydraulic pressure. (b) Crack dilation in the surrounding rock. (c) Crack network and leakage. (d) Water inrush.

excavation disturbance, structural characteristics of rock mass, and discontinuous surfaces such as bedding, joints, and fissures are ignored [3, 4, 28, 29]. In fact, the rock in karst strata has an obvious bedding structure such as foliated rock, and there is a set of joints orthogonal to the bedding, as shown in Figure 3. The left side of Figure 3 shows the structural characteristics of limestone in the karst area and the spatial relationship between karst water cavities and tunnels. The right side of Figure 3 is a schematic diagram of the water inrush disaster process of the karst tunnel under the disturbance of blasting excavation. As shown in Figure 3, the process of water inrush disaster is the result of the initiation, expansion, and penetration of the initial discontinuity under the combined action of blasting excavation and karst water pressure. Moreover, most of the existing studies simplify the karst shape into circular (two-dimensional) or spherical (three-dimensional) holes, which are far from the actual karst shape. So, in order to better simulate and analyze the dynamic evolution process of information characteristics, this paper uses the discrete element software that can consider the blasting excavation effect and crack development, simplify the karst cavity into an ellipse, and perform a series of numerical simulations about karst tunnel water inrush implements.

2.2.2. Numerical Model and Boundary Conditions. The calculation size of the model is 80 m × 80 m, the cross-section of the tunnel is a three-centered circle, the height of the tunnel is 9.5 m, the tunnel span is 8.5 m, and the tunnel depth is 500 m. The hidden cavity above the tunnel is simplified to an ellipse with a 20 m long axis and a 12 m short axis, and the thickness of the outburst prevention layer between the tunnel and the cavity is 3 m. The thickness of the layered rock mass is 1 m, with a total of 80 layers (as shown in Figure 4).

According to the tunnel depth, the weight of the overlying rock is converted into a vertical uniform load and applied to the top boundary of the model. The left, right, and upper boundaries of the model are stress boundaries, and the values are $kq_0 + \gamma h$, $kq_0 + \gamma h$, and kq_0, respectively. The bottom boundaries of the model are set as fixed boundaries. The karst water pressure is 1 MPa and the lateral pressure coefficient (k) is 1.2, as shown in Figure 5. The mechanical properties of the numerical model are determined by the mechanical parameters of the blocks and the mechanical properties of the joints between the blocks. Since the block material is regarded as a large number of deformed microblocks, in order to balance the accuracy of the calculation. Therefore, the Mohr-Coulomb model (The

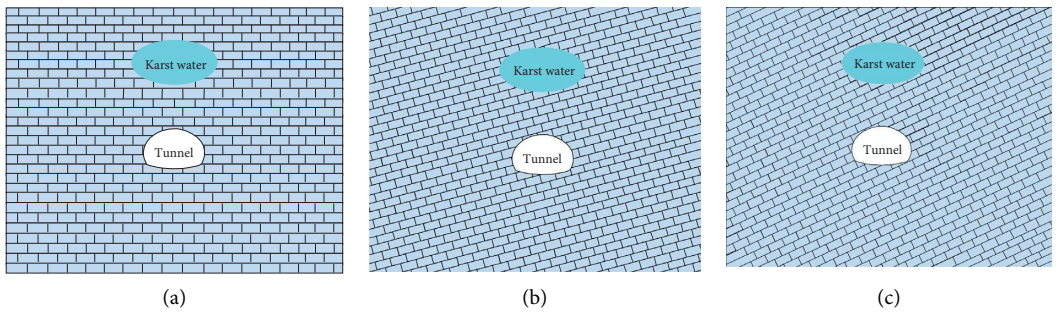

Figure 4: Simulation calculation model. (a) $\theta = 0^{\circ}$. (b) $\theta = 15^{\circ}$. (c) $\theta = 30^{\circ}$.

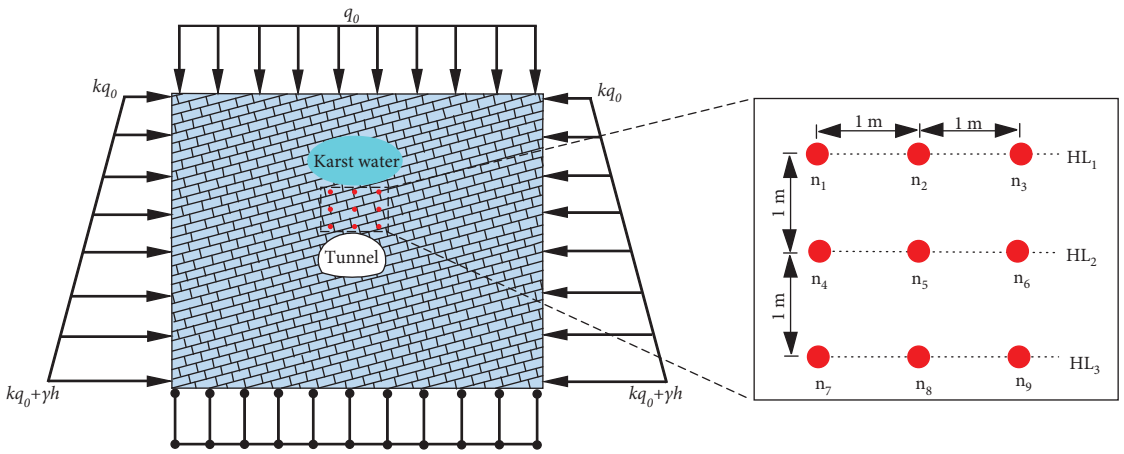

Figure 5: Boundary conditions and measuring points arrangement.

Table 1: Block and joint mechanical parameters in numerical simulation [32].

Material	Unit weight	Elastic bulk modulus	Poisson's ratio	Friction angle	Cohesion (MPa)	Normal stiffness	Tangential stiffness
Block	24 kN/m^3	30 GPa	0.25	35°	0.8	—	—
Joint	—	—	—	33°	0.5	180 GPa/m	144 GPa/m

cons = 2) is used for the water and mud-resistant rock mass in the tunnel face; the Coulomb sliding model (The *j*cons = 1) is used for the layered joints. The mechanical parameters of the blocks and joints in the model are shown in Table 1. Nine measuring points were set up to obtain the variation law of displacement and water pressure in the water and mud-resistant rock mass under the action of blasting excavation and high karst water pressure, as shown in Figure 5. In the process of dynamic calculation, the model boundary is a nonreflective boundary. According to the research literature [30, 31], the blasting load curve is triangular, and the peak value of the equivalent blasting load is 30 MPa. The load rise time is 0.009 s, and the positive pressure action time is 0.04 s.

2.2.3. Numerical Simulation Scheme. According to the existing research [33–35], the layered joints angle, the tunnel depth, and the outburst prevention rock thickness have an important impact on the stability of the surrounding rock in karst tunnels. Therefore, this paper designs the simulation scheme shown in Table 2 to study the influence of these influencing factors on the catastrophic mechanism of water inrush in karst tunnel.

3. Simulation Results and Discussion

3.1. Catastrophe Information of Water Inrush in Karst Tunnel under Different Joint Inclination Angles

3.1.1. Evolution Characteristics of Displacement under Different Joint Inclination Angles. Figure 6 is the evolution process of the displacement values of the water and mud resistant rock mass under the conditions that the tunnel depth is 500 m, the thickness of water and mud resistant rock mass is 3 m, and the joint inclination angles are 0°, 15°, and 30°, respectively.

Under the continuous action of blasting load, the water and mud-resistant rock masses located at different joint inclination angles have different degrees of displacement. When the inclination angle of the joint is 0°, the surrounding rock of the tunnel is in a stable state as a whole, and the vertical displacement of the water and mud-resistant rock mass is relatively small (At $t = 7$s, the displacement is

Table 2: Numerical calculation scheme.

Number	Influencing factors		
	Joint inclination (°)	Tunnel depth (m)	The thickness of water and mud-resistant rock mass (m)
1	0	500	3
2	15	500	3
3	30	500	3
4	15	200	3
5	15	500	3
6	15	800	3
7	15	500	2
8	15	500	3
9	15	500	4

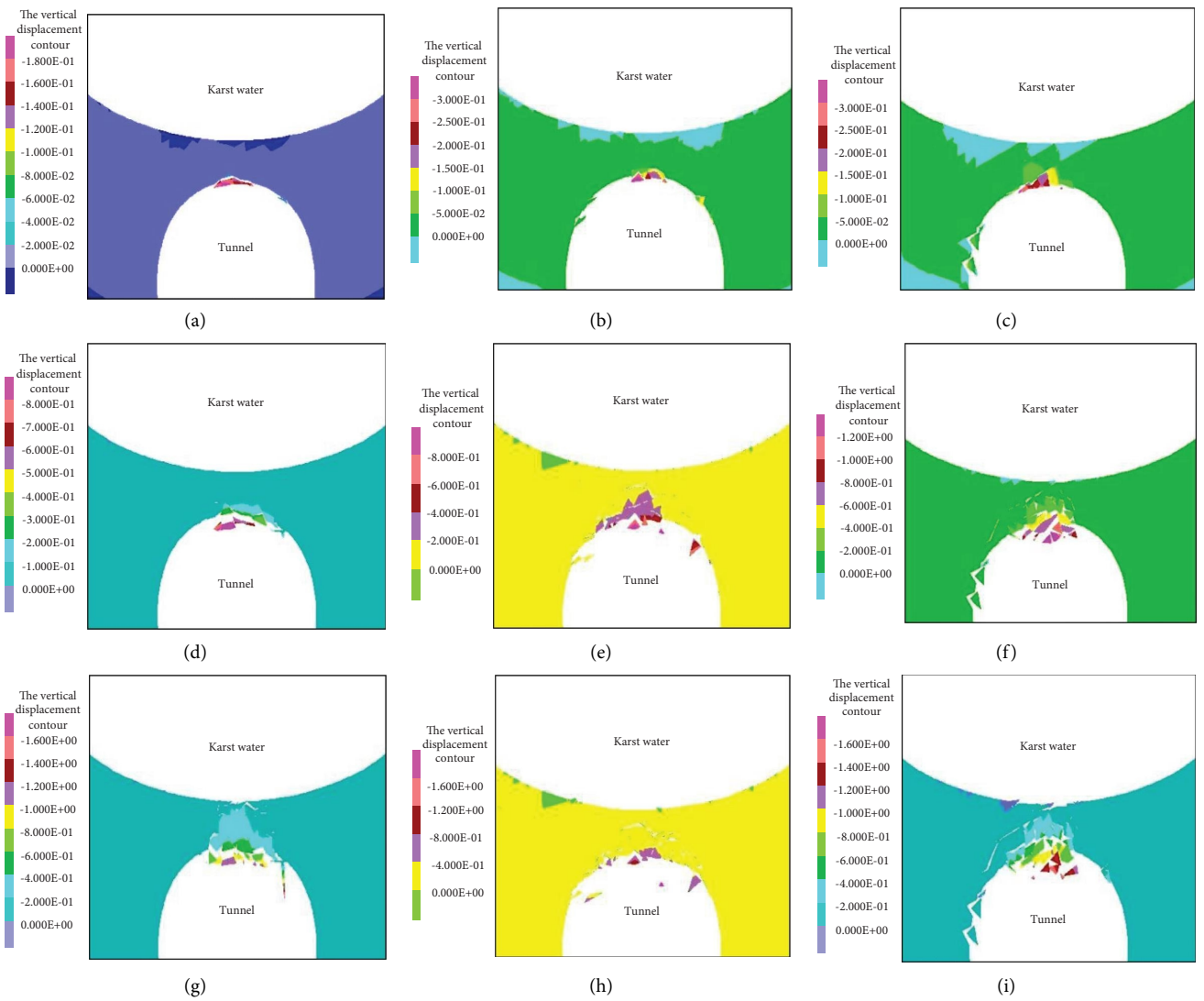

Figure 6: Continued.

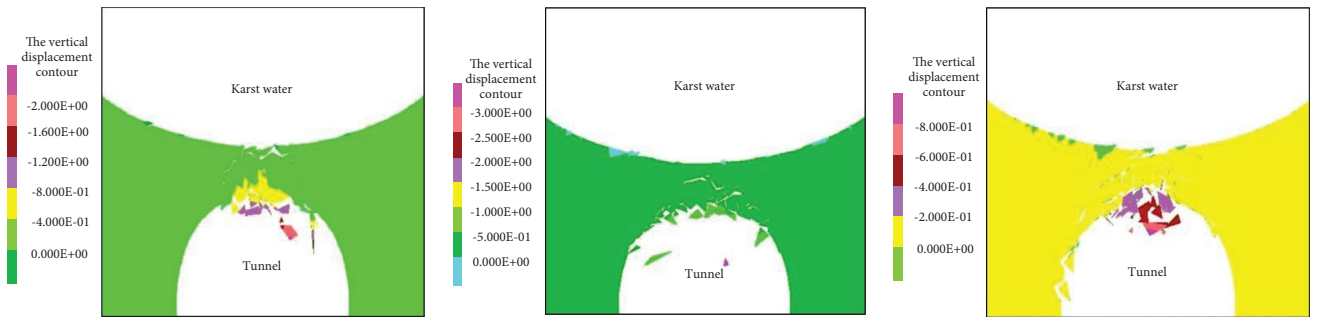

FIGURE 6: Evolution characteristics of displacement under different joint inclination angles. (a) $t = 1$ s, $\theta = 0^{\circ}$. (b) $t = 1$ s, $\theta = 15^{\circ}$. (c) $t = 1$ s, $\theta = 30^{\circ}$. (d) $t = 3$ s, $\theta = 0^{\circ}$. (e) $t = 3$ s, $\theta = 15^{\circ}$. (f) $t = 3$ s, $\theta = 30^{\circ}$. (g) $t = 5$ s, $\theta = 0^{\circ}$. (h) $t = 5$ s, $\theta = 15^{\circ}$. (i) $t = 5$ s, $\theta = 30^{\circ}$. (j) $t = 7$ s, $\theta = 0^{\circ}$. (k) $t = 7$ s, $\theta = 15^{\circ}$. (l) $t = 7$ s, $\theta = 30^{\circ}$.

−0.34 m; the negative sign indicates that the displacement is vertically downward in the y-direction). However, as the inclination angle of the joints increased to 15° and 30°, the fracture degree and vertical displacement in the water and mud-resistant rock mass increased significantly (At $t = 7$ s, the displacements are −0.56 m and −0.64 m, an increase of 64.7% and 88.2%, respectively). The reason is that the increase of the inclination angle of the joints reduces the stability of the surrounding rock. Under the combined action of blasting and excavation disturbance and joint inclination, the stress stored in the surrounding rock is further released, and the cracks in the rock stratum rapidly sprout and expand, resulting in further expansion of the damaged area. Especially when the inclination angle of the joint is 30°, there are obvious blocks falling off, and the number and connectivity of the cracks in the water and mud-resistant rock mass increase rapidly, which makes the instability of the water and mud-resistant rock mass rapidly increase. Therefore, the higher the inclination angle of the joints, the more unstable the water and mud resistant rock mass is, and the more significant the effects of blasting load are, the more serious the fracture of the water and mud resistant rock mass is, the weaker the antioutburst ability, and the more prone to water inrush in the tunnel.

Figure 7 shows the evolution process of the vertical displacement of each measuring point in the water and mud-resistant rock mass. Comparing the vertical displacement of each measuring point at the same joint inclination angle, it can be seen that the displacement change values increase significantly with the increase of blasting action time, and the displacement change values of the measuring points that are close to the tunnel excavation surface are significantly higher those that of other measuring points. Taking the joint inclination angle $\theta = 15^{\circ}$ and selecting the measuring points n_7-n_9 on HL_3 as an example, when the blasting load action time $t = 1$ s, the y-direction displacement values are −0.025 m, −0.223 m, −0.179 m (the negative sign indicates that the displacement is vertically downward in the y-direction); when the blasting load action time $t = 5$ s, the y-direction displacements values are −0.284 m, −0.489 m, −0.463 m. With the continuous action of the blast stress wave, the cracks in the water and mud-resistant rock mass quickly initiate, expand, and penetrate each other, which makes the displacement of the measuring point on the side close to the tunnel profile increase significantly. At the same time, the displacement of n_8 on the measuring surface HL_3 is higher than that of n_7 or n_9, and correspondingly, the vertical displacement growth of n_3 and n_5 on HL_1 and HL_2 is higher. This shows that the degree of fragmentation at the vault of the tunnel is relatively serious during the blasting excavation process.

3.1.2. Evolution Characteristics of Seepage Pressure under Different Joint Inclination Angles. Figure 8 shows the evolution characteristics of seepage pressure value of the water and mud resistant rock mass under different joint inclination angles when the tunnel depth is 500 m, the thickness of water and mud resistant rock mass is 3 m. The joint inclination angles of the three columns in Figure 8 are 0°, 15°, and 30°, respectively.

It can be seen from Figure 8 that with the continuous increase of the inclination angle of the joints, the seepage area and the expansion degree of the cracks in the water and mud-resistant rock mass increase significantly under the continuous action of the blasting load. Before the tunnel is excavated, a stable seepage field has been formed near the cavity. The blasting and unloading of the surrounding rock induce significant changes in the seepage field, especially in the water and mud-resistant rock mass between the cavern and the tunnel. When the inclination angle of the joint is 0°, under the dual action of karst water pressure and blasting excavation disturbance, relatively few cracks are generated in the upper and middle parts of the water and mud-resistant rock mass, and the cracks do not extend to the tunnel vault, and the macro water inrush channel is not formed ($t = 7$ s). With the continuous increase of the inclination angle of the joints, under the influence of the explosion stress wave, the seepage damage of the rock mass is gradually intensified, and the surrounding rock continues to have crack initiation and expansion ($\theta = 15^{\circ}$, $t = 7$ s). When the inclination angle of the joint increases to 30°, the stability of the water and mud-resistant rock mass is further reduced. Under the continuous action of the blasting load, its internal cracks rapidly expand

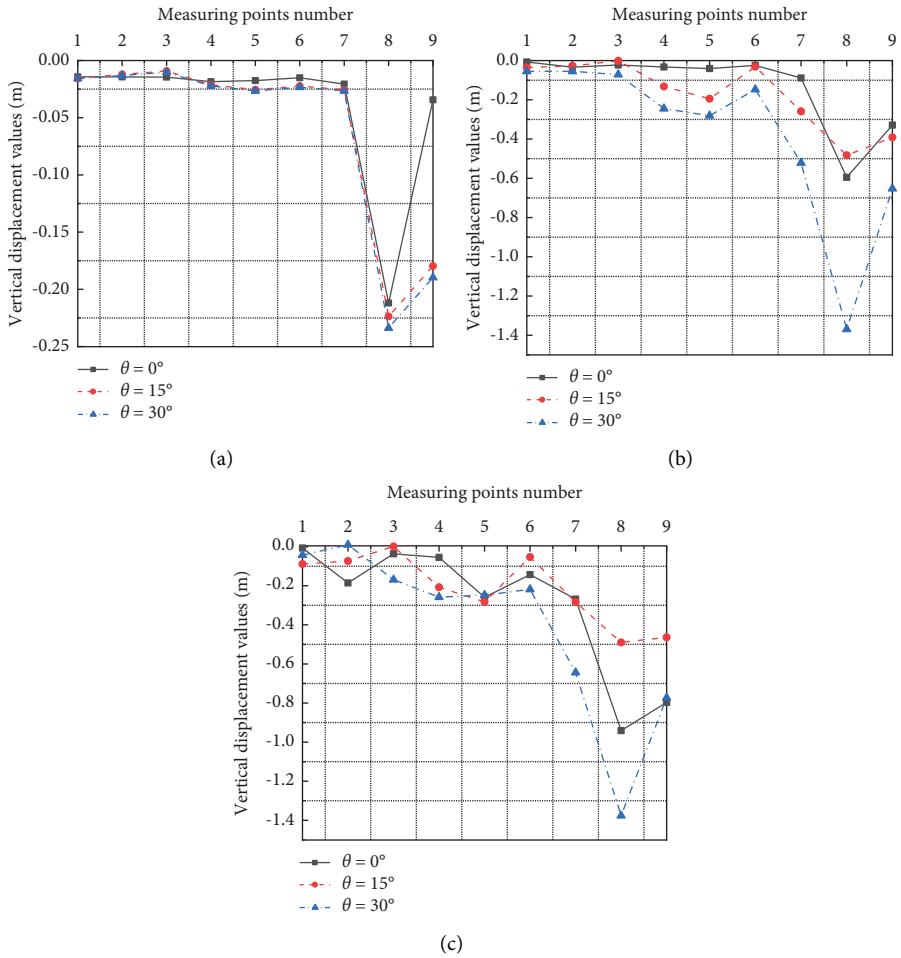

Figure 7: Evolution characteristics of displacement in the measuring points. (a) $t = 1$ s. (b) $t = 3$ s. (c) $t = 5$ s.

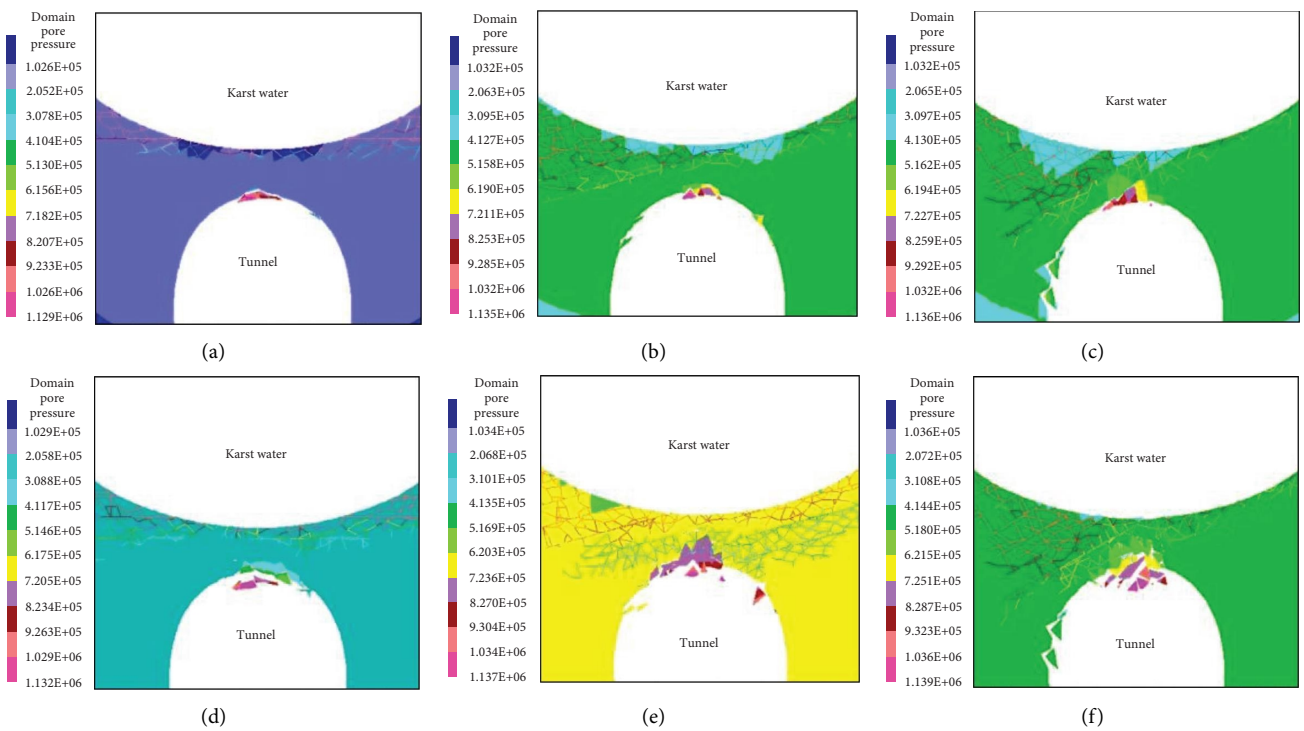

Figure 8: Continued.

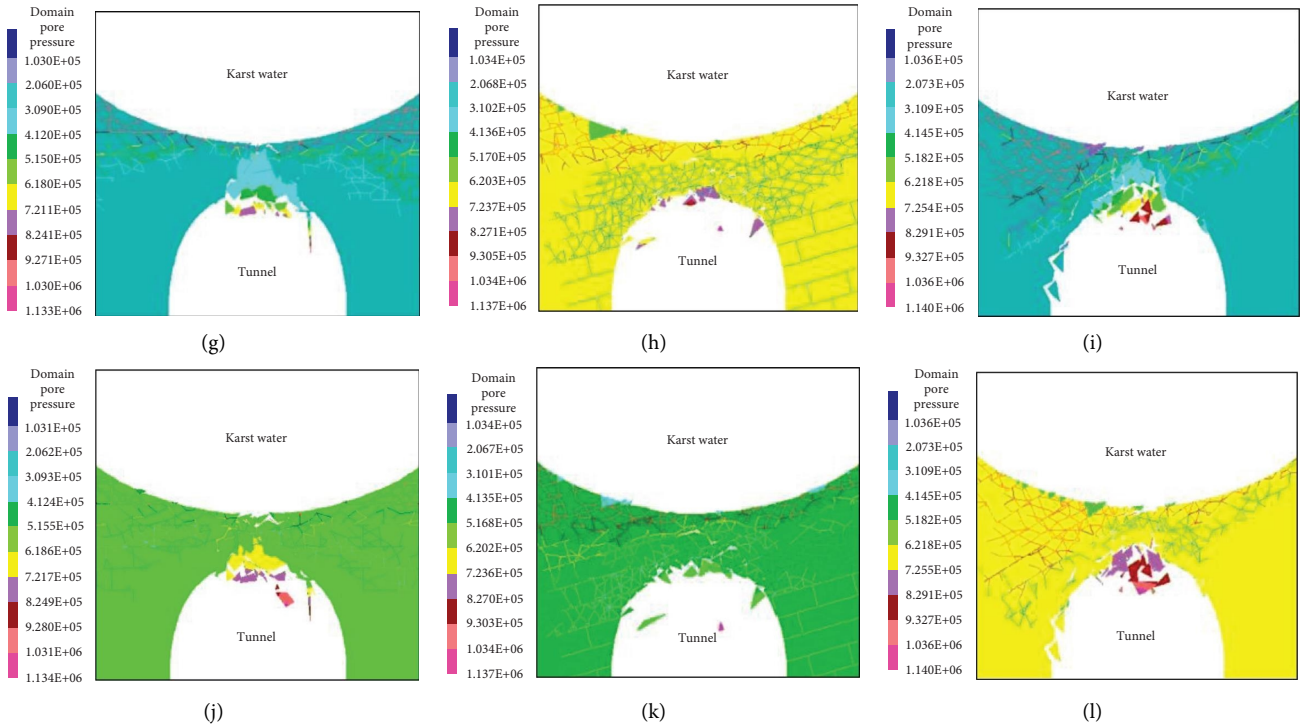

FIGURE 8: Evolution characteristics of seepage pressure under different joint inclination angles.(a) $t = 1$ s, $\theta = 0^{\circ}$. (b) $t = 1$ s, $\theta = 15^{\circ}$. (c) $t = 1$ s, $\theta = 30^{\circ}$. (d) $t = 3$ s, $\theta = 0^{\circ}$. (e) $t = 3$ s, $\theta = 15^{\circ}$. (f) $t = 3$ s, $\theta = 30^{\circ}$. (g) $t = 5$ s, $\theta = 0^{\circ}$. (h) $t = 5$ s, $\theta = 15^{\circ}$. (i) $t = 5$ s, $\theta = 30^{\circ}$. (j) $t = 7$ s, $\theta = 0^{\circ}$. (k) $t = 7$ s, $\theta = 15^{\circ}$. (l) $t = 7$ s, $\theta = 30^{\circ}$.

and penetrate to form a macroscopic water inrush channel; the rapid inflow of karst water into the tunnel further destabilizes the water and mud-resistant rock mass; and the water inrush disaster occurs in the karst tunnel ($t = 7$ s). Therefore, the higher the inclination angle of the rock joints is, under the combined action of the continuous disturbance of blasting excavation and the karst water pressure, the primary fissures in the water and mud-resistant rock mass are easy to develop and penetrate, thus forming the water inrush channel.

Figure 9 shows the evolution process of seepage water pressure at each measuring point in the water and mud-resistant rock mass under different joint dip angles. Under the dual action of blasting and excavation disturbance and karst water pressure, the seepage pressure for each measuring point in the water and mud resistant rock mass gradually increased and showed a decreasing trend from top to bottom along the water and mud resistant rock mass. Since the measuring surface HL_1 is close to the karst cavity, the seepage pressures of the n_1-n_3 measuring points quickly reach the karst water pressure of 1 MPa ($\theta = 0^{\circ}$, 15°, and 30°). Under the continuous action of the blasting load, the fissures in the water and mud-resistant rock mass gradually expand and penetrate, and the karst water gradually penetrates the fissures under the action of hydraulic pressure. When the seepage pressure exceeds the critical fracture pressure of the fracture, the fracture begins to initiate and expand, and these fractures can extend to the $n_1 \sim n_6$ measuring points. Therefore, no matter whether the joint inclination angle is 0°, 15°, or 30°, it can be seen from Figure 8 that the seepage pressure values of the measuring points $n_1 \sim n_6$ are much higher than the seepage pressure values of $n_7 \sim n_9$ at the bottom of the water and mud-resistant rock mass. When the inclination of the joint is 0°, the water pressure of n_4-n_6 is 0.12 MPa, 0.10 MPa, and 0.19 MPa, respectively (at $t = 3$ s); When the inclination of the joint is 0°, the water pressure of n_4-n_6 is 0.64 MPa, 0.45 MPa, 0.52 MPa (at $t = 3$ s), respectively. It shows that due to the influence of the joint dip angle, the surrounding rock structure is unstable and prone to cracks, and the karst water easily penetrates into the aquifer, which increases the seepage pressure value and forms a wider range of seepage.

3.2. Catastrophe Information of Water Inrush in Karst Tunnel under Different Tunnel Depths

3.2.1. Evolution Characteristics of Displacement under Different Tunnel Depths. Figure 10 is the evolution process of the displacement value of the water and mud resistant rock mass under the conditions of joint inclination angle $\theta = 15^{\circ}$, the water and mud resistant rock mass are 3 m, the pressure of karst water is 2 MPa, and the depth of tunnel is 200 m, 500 m, and 800 m, respectively.

It can be seen from Figure 10 that the water and mud-resistant rock masses of karst tunnels in different burial depths are damaged to varying degrees and have obvious blocks falling under the disturbance of blasting excavation. When the buried depth of the tunnel is 200 m, with the increase of blasting load action time, the stability of the water

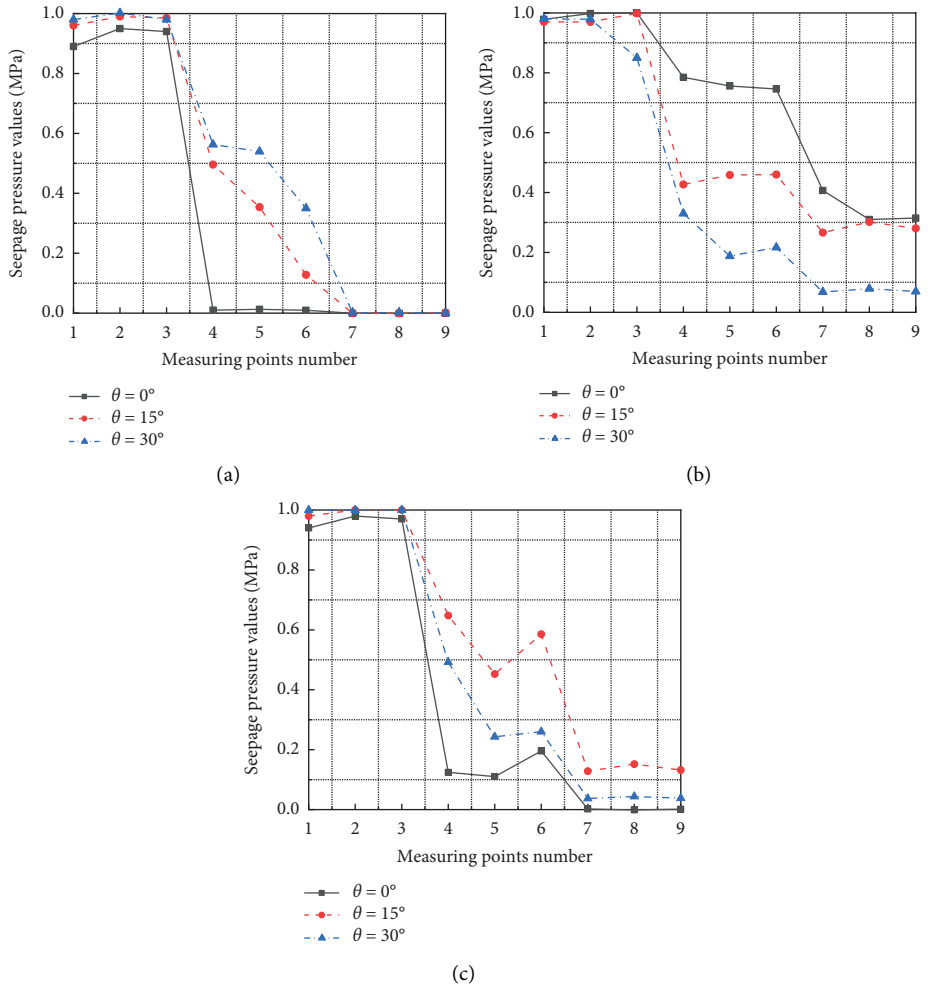

Figure 9: Evolution characteristics of seepage pressure in the measuring points.(a) $t = 1$ s. (b) $t = 3$ s. (c) $t = 5$ s.

and mud resistant rock mass gradually decreases, and the rock mass at the lower part of the water and mud resistant rock mass gradually collapses in a high area. When the blasting time $t = 7$ s, the entire water and mud-resistant rock mass is almost destroyed and some blocks fall to the bottom of the tunnel. When the buried depth of the tunnel is 500 m, the vertical displacement of the water and mud-resistant rock mass is relatively reduced, and the stability of the structure is enhanced. Although some blocks fell, the scale of the rock mass was reduced, and the water and mud-resistant rock mass did not completely collapse. When the depth of the tunnel was 800 m, the structural stability of the aquifer was the best. Although some of the blocks fell, the size of the blocks and the degree of fragmentation for the water and mud-resistant rock mass were relatively reduced. When the blasting time $t = 7$ s, the remaining complete thickness of the water and mud-resistant rock mass is the largest, and no obvious crack channel is formed in the rock layer. The numerical calculation results fully show that under the continuous action of blasting load, with the increase of tunnel burial depth, the stability of the water and mud-resistant rock mass and the ability to resist water inrush are gradually enhanced.

Figure 11 shows the evolution process of the vertical displacement of each measuring point located in the water and mud-resistant rock mass under the condition that the tunnel depth is 200 m, 500 m, and 800 m, respectively. It can be seen from Figure 11 that the vertical displacement change value and growth rate of each measuring point are different at different tunnel depths. When the depth of the tunnel is 200 m, the blasting action time is $t = 1$ s, 3 s, and 5 s, respectively, and the maximum displacement of each measuring point is −0.26 m, −1.08 m, −1.85 m (the negative sign indicates that the displacement is vertically downward in the y-direction), the displacement change value is significantly higher than the buried depth of 500 m and 800 m. This shows that the greater the buried depth of the tunnel, the stronger the overall stability of the water and mud-resistant rock mass, which can reduce the negative effect of blasting load on it. With the increase of blasting action time (at $t = 5$ s), the vertical displacement growth value of each measuring point on the measuring surfaces HL_1 and HL_2 decreases relatively, and the changing trend of each measuring point is relatively uniform. The vertical displacement growth value of each measuring point on HL_3 is relatively significant, indicating that the blasting excavation disturbance has a limited impact on the surrounding rock of

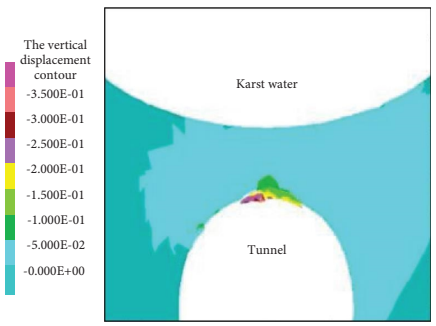

(a)

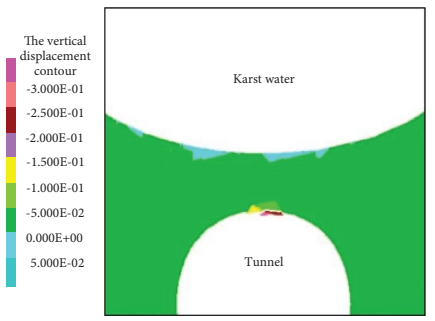

(b)

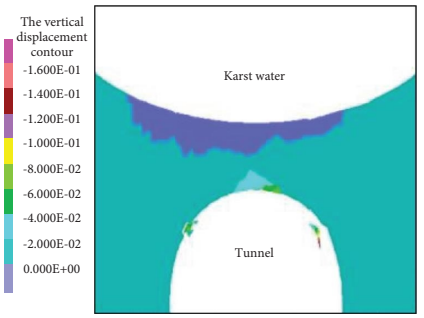

(c)

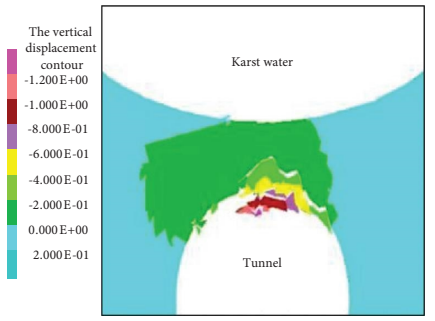

(d)

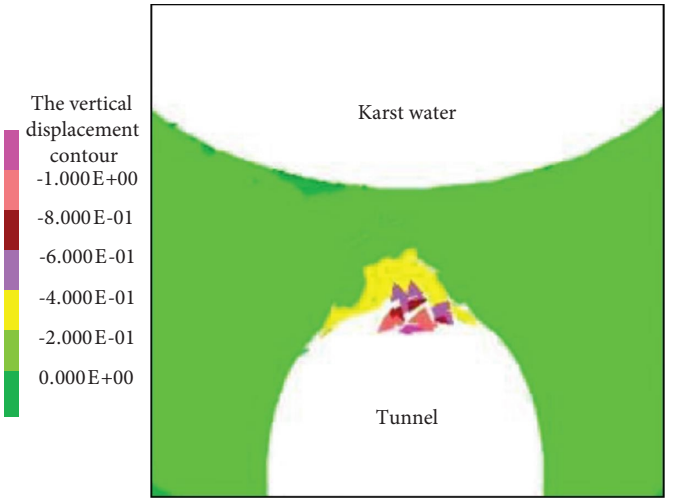

(e)

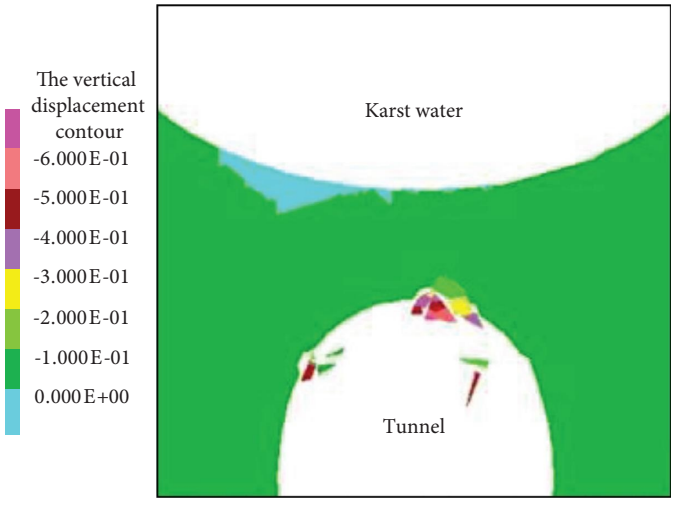

(f)

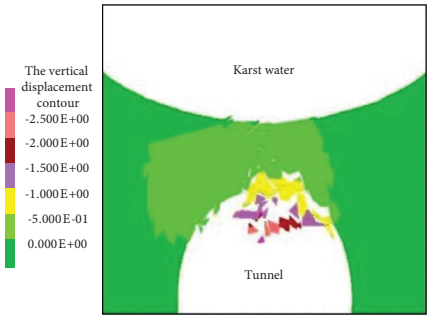

(g)

Figure 10: Continued.

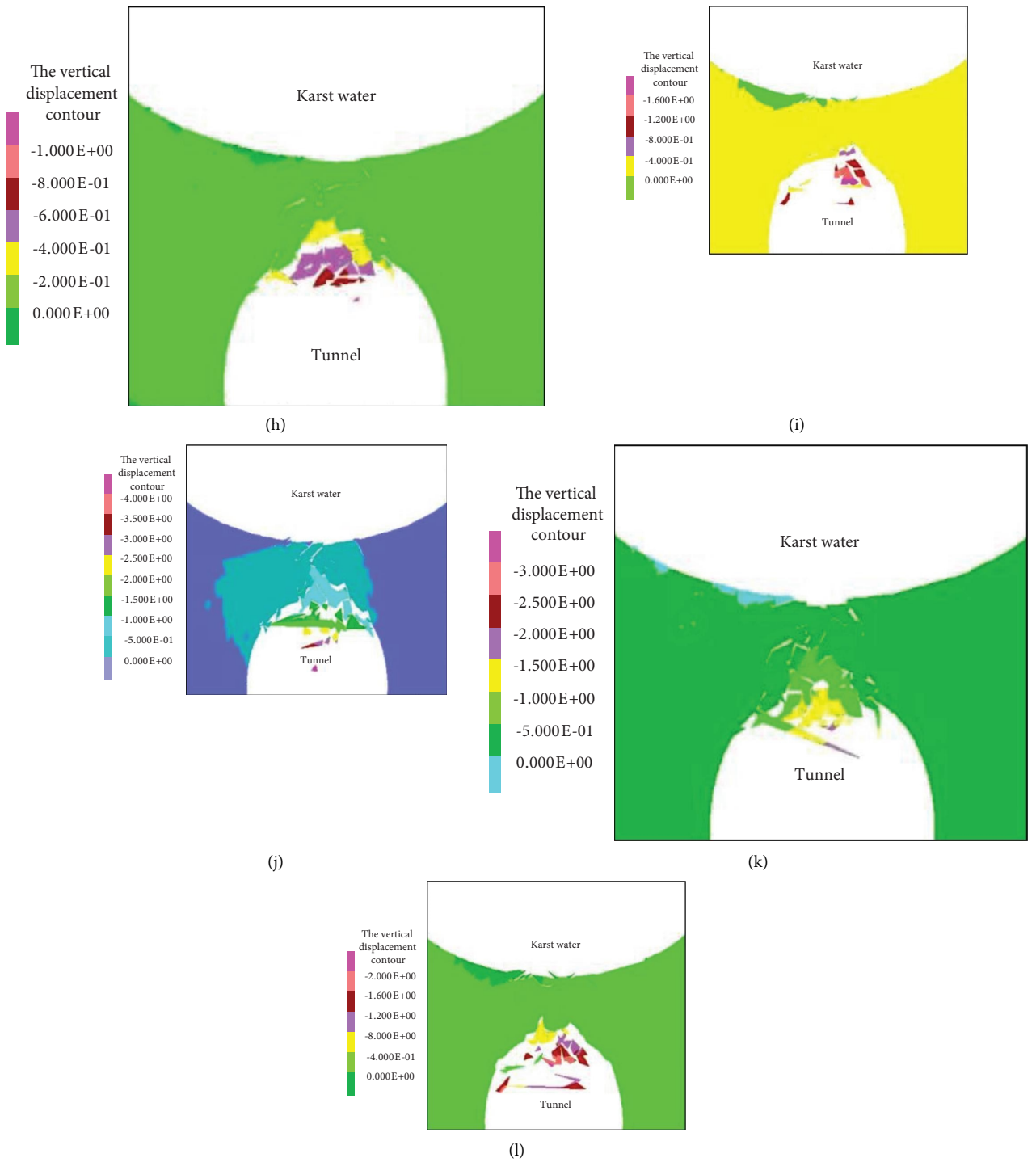

Figure 10: Evolution characteristics of displacement under different tunnel depths. (a) $t = 1$ s, $h = 200$ m. (b) $t = 1$ s, $h = 500$ m. (c) $t = 1$ s, $h = 800$ m. (d) $t = 3$ s, $h = 200$ m. (e) $t = 3$ s, $h = 500$ m. (f) $t = 3$ s, $h = 800$ m. (g) $t = 5$ s, $h = 200$ m. (h) $t = 5$ s, $h = 500$ m. (i) $t = 5$ s, $h = 800$ m. (j) $t = 7$ s, $h = 200$ m. (k) $t = 7$ s, $h = 500$ m. (l) $t = 7$ s, $h = 800$ m.

the tunnel and has a greater impact on the surrounding rock structure of the adjacent tunnel.

3.2.2. Evolution Characteristics of Seepage Pressure under Different Tunnel Depths. Figure 12 shows the evolution process of the seepage field of the water and mud resistant rock mass under the conditions of the karst water pressure of 2 MPa, the thickness of water and mud resistant rock mass is 3 m, the joint inclination angle is 15°, and the tunnel depth is 200 m, 500 m, and 800 m, respectively.

Similar to the evolution process of the seepage field of the water and mud-resistant rock mass in Section 3.1.2, the karst water gradually infiltrated the vault and spandrel of the

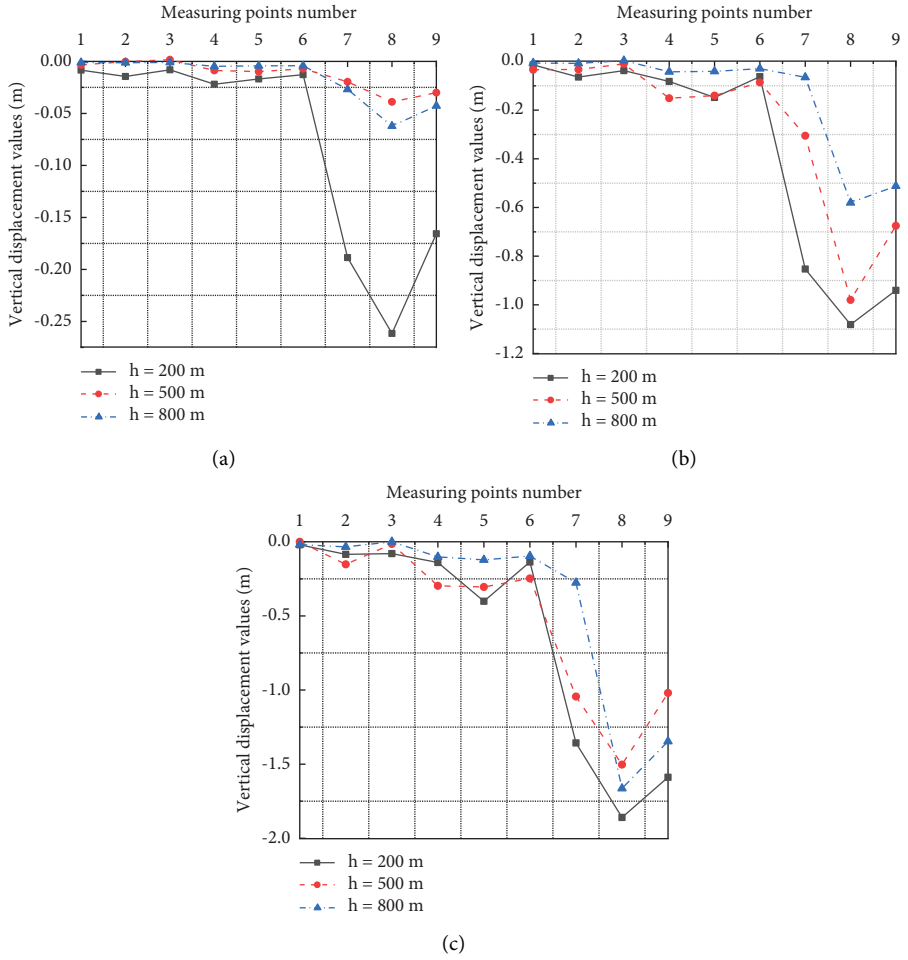

Figure 11: Evolution characteristics of displacement in the measuring points.(a) $t = 1$ s. (b) $t = 3$ s. (c) $t = 5$ s.

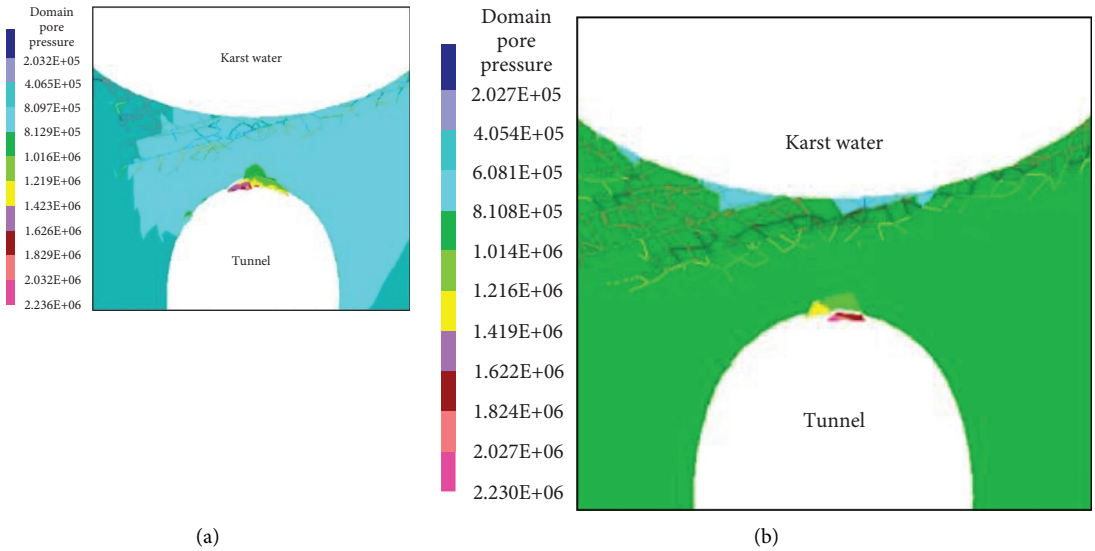

Figure 12: Continued.

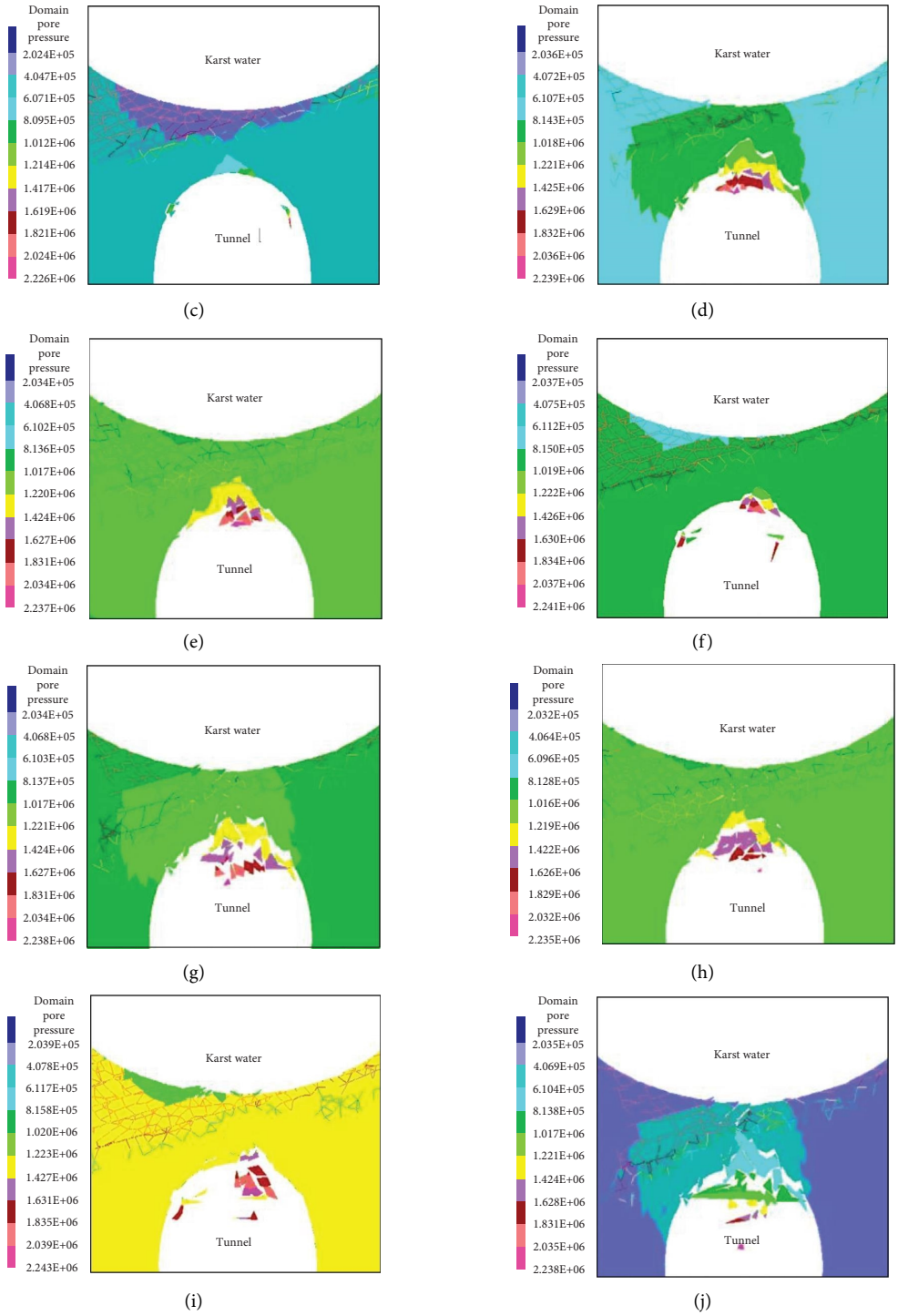

Figure 12: Continued.

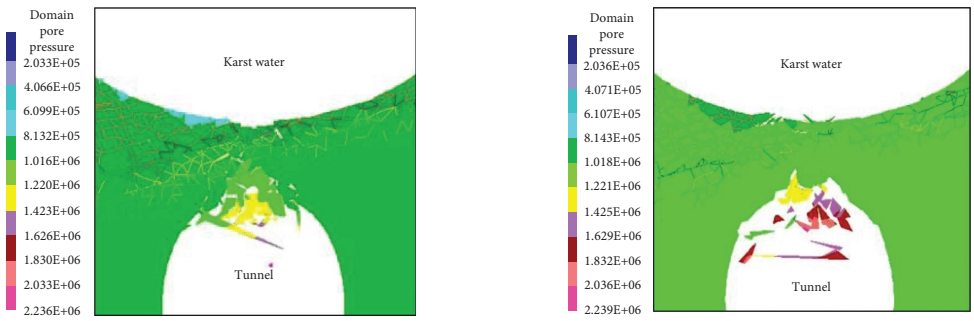

FIGURE 12: Evolution characteristics of seepage pressure under different tunnel depths. (a) $t = 1$ s, $h = 200$ m. (b) $t = 1$ s, $h = 500$ m. (c) $t = 1$ s, $h = 800$ m. (d) $t = 3$ s, $h = 200$ m. (e) $t = 3$ s, $h = 500$ m. (f) $t = 3$ s, $h = 800$ m. (g) $t = 5$ s, $h = 200$ m. (h) $t = 5$ s, $h = 500$ m. (i) $t = 5$ s, $h = 800$ m. (j) $t = 7$ s, $h = 200$ m. (k) $t = 7$ s, $h = 500$ m. (l) $t = 7$ s, $h = 800$ m.

tunnel through the fissures in the water and mud-resistant rock mass. Due to the difference in tunnel depth, the seepage velocity of karst fissure water and the propagation velocity of fissures are different. When the buried depth of the tunnel is 200 m, under the continuous action of the blasting load, the water and mud-resistant rock mass rapidly develop and penetrate to form an obvious water inrush channel (at $t = 1 \sim 7$ s). When the buried depth of the tunnel is 500 m, the development speed of cracks in the water and mud-resistant rock mass decreases somewhat (at $t = 1 \sim 7$ s). When the buried depth of the tunnel is 800 m, no obvious crack water inrush channel is formed in the water and mud-resistant rock mass (at $t = 1 \sim 7$ s). In addition, it can be seen that the distribution area of the seepage area for the tunnel's surrounding rock in the water and mud-resistant rock mass decreases significantly with the increase of the tunnel depth. When the blasting time $t = 7$ s, the degree of fracture and the scale of water inrush in the water and mud-resistant rock mass of the tunnel surrounding rock with a buried depth of 200 m reach their maximum in the above three cases. This phenomenon shows that under the combined action of hydraulic pressure and blasting excavation disturbance, the smaller the tunnel depth, the greater the disturbance of the water and mud-resistant rock mass by blasting load, and the easier it is to form higher cracks, which will speed up the formation of water inrush channels and the occurrence of water inrush disasters.

Figure 13 shows the evolution process of the seepage pressure value at each measuring point of the water and mud-resistant rock mass of karst tunnels with different burial depths under blasting excavation. It can be seen from Figure 13 that the seepage pressure values of the $n_1 \sim n_3$ measuring points on the horizontal plane HL_1 can reach the karst water pressure of 2 MPa in a very short time under the conditions of different burial depths ($h = 200$ m, 500 m, and 800 m). When the buried depth of the tunnel is 200 m, the seepage pressure values of n_4-n_9 measuring points in the water and mud-resistant rock mass decrease with the increase of blasting time (At $t = 1$ s, the measuring points of n_4-n_6 are 0.74 MPa, 0.58 MPa, and 0.18 MPa; At $t = 3$ s, the measuring points of n_4-n_6 are 0.440 MPa, 0.06 MPa, and 0.05 MPa; At $t = 5$ s, the measuring points of n_4-n_6 are 0.62 MPa, 0.37 MPa, and 0.03 MPa). The reason for this phenomenon is that the continuous disturbance of blasting excavation accelerates the formation of water inrush channels in the cracks. Therefore, the water pressure at each measuring point in the water and mud-resistant rock mass has decreased. When the buried depth of the tunnel is 500 m and 800 m respectively, the seepage pressure value at each measuring point of HL2 and HL3 increases to varying degrees. This is because the stability of the aquifer structure gradually increases with the increase in the buried depth of the tunnel, and the effect of blasting excavation disturbance is weakened. There is no obvious crack channel in the aquifer, and the energy loss of karst water in the flow process is less. Therefore, the seepage pressure values of the $n4$-$n6$ measuring points have increased.

3.3. Catastrophe Information of Water Inrush in Karst Tunnel under Different Thickness

3.3.1. Evolution Characteristics of Displacement under Different Thickness. Figure 14 shows the evolution process of the displacement values of the water and mud-resistant rock mass under the conditions of the karst water pressure is 1 MPa, the inclination of the joint is 15°, the tunnel depth is 500 m, and the thicknesses of water and mud-resistant rock mass are 2 m, 3 m, and 4 m, respectively.

The process of water inrush disaster in the water and mud-resistant rock mass based on the displacement values evolution in Figure 14 is roughly similar to that in Figures 6 and 10, but due to the different thickness of the water and mud-resistant rock mass, the evolution characteristics of each displacement value are significantly different (the negative sign indicates that the displacement is vertically downward in the y-direction). With the increase in the calculation time, the broken area in the water and mud-resistant rock mass gradually expands to the upper part in different thicknesses of water and mud-resistant rock mass. When the thickness of the water and mud resistant rock mass is 2 m, the structure of the water and mud resistant

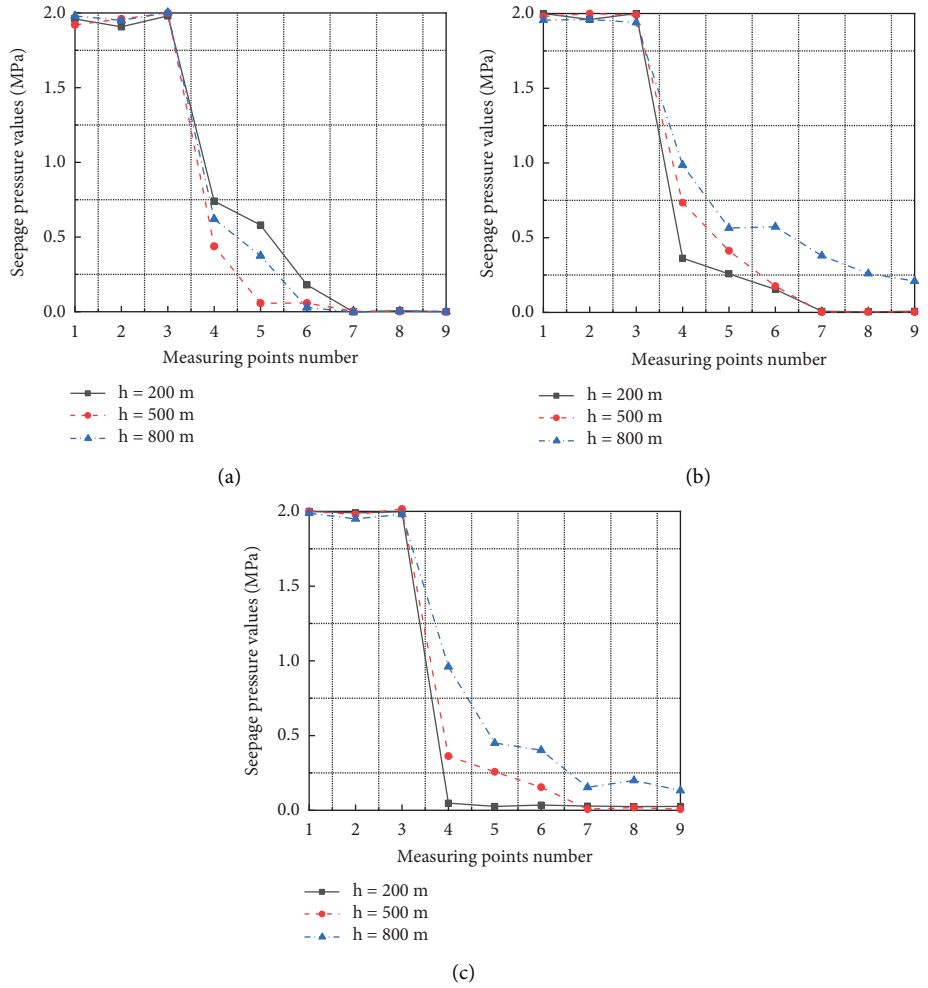

Figure 13: Evolution characteristics of seepage pressure in the measuring points. (a) $t = 1$ s. (b) $t = 3$ s. (c) $t = 5$ s.

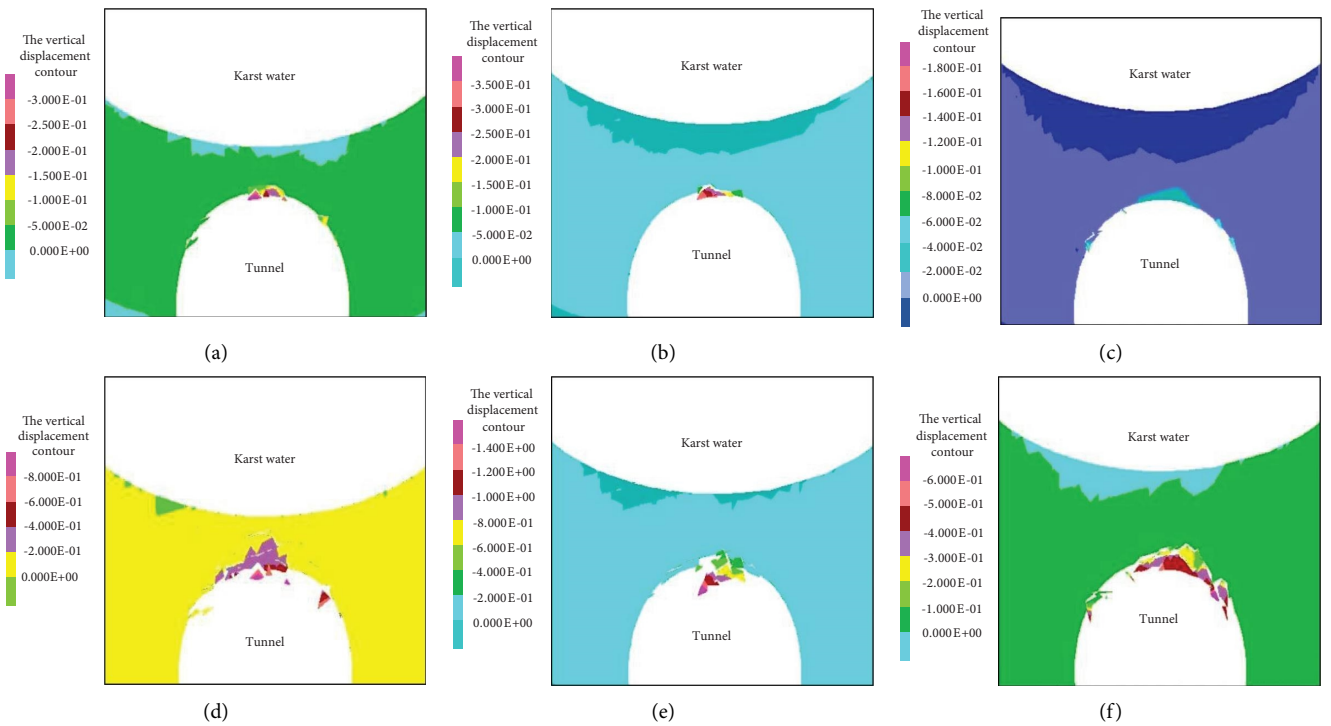

Figure 14: Continued.

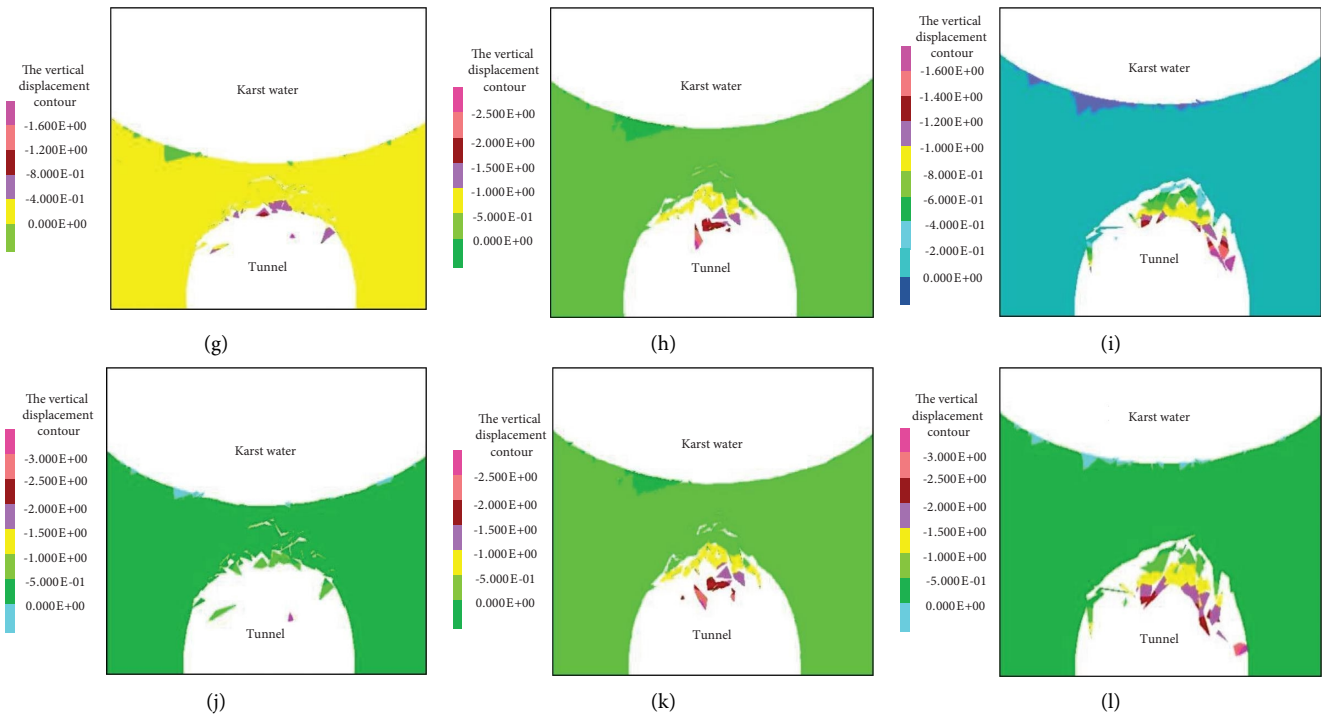

FIGURE 14: Evolution characteristics of displacement under different thicknesses.(a) $t = 1$ s, $d = 2$ m. (b) $t = 1$ s, $d = 3$ m. (c) $t = 1$ s, $d = 4$ m. (d) $t = 3$ s, $d = 2$ m. (e) $t = 3$ s, $d = 3$ m. (f) $t = 3$ s, $d = 4$ m. (g) $t = 5$ s, $d = 2$ m. (h) $t = 5$ s, $d = 3$ m. (i) $t = 5$ s, $d = 4$ m. (j) $t = 7$ s, $d = 2$ m. (k) $t = 7$ s, $d = 3$ m. (l) $t = 7$ s, $d = 4$ m.

rock mass shows an overall layer-wise failure trend under the action of excavation disturbance. With the continuous increase of the thickness of water and mud-resistant rock mass, the surrounding rock located within 1.5 m of the tunnel vault suffered severe damage along the way, resulting in the formation of obvious slump arches. It can also be seen from the calculation results in Figure 13 that when the thickness of the water and mud-resistant rock mass is 2 m, the structure of the antioutburst rock mass undergoes significant displacement, the entire structure is severely broken, and obvious crack channels have been formed inside. When the thickness of the water and mud resistant rock mass increases to 3 m and 4 m, although some blocks fall off, the remaining structure of the water and mud resistant rock mass is relatively complete, and no obvious crack channel is formed. It can be seen that with the continuous increase of the safety thickness of the water and mud resistant rock mass, the stronger the stability of the water and mud resistant rock mass, the higher the critical water pressure when water inrush occurs.

Figure 15 shows the evolution process of the vertical displacement of each measuring point in different water and mud-resistant rock mass thicknesses. It can be seen from the results in Figure 15 that in the case of any thickness of the water and mud resistant rock mass (2 m, 3 m, and 4 m), the y-direction displacement of the water and mud resistant rock mass gradually increases with the increase of the blasting load action time. And it can be seen from Figure 15 that the y-direction displacement of the antioutburst layer gradually increases from top to bottom along its thickness. The thickness of the antiburst layer is 3 m as an example, and the measuring points n_7, n_8, and n_9 are selected. When the blasting action time $t = 3.0$ s, the y-direction displacements are −0.412 m, −0.557 m, and −0.464 m, respectively (The negative sign indicates that the displacement is vertically downward in the y-direction). When the blasting action time $t = 5.0$ s, the y-direction displacement is 0.896 m, 1.359 m, and 0.996 m, and the displacement increases downward by 117.4%, 143.9%, and 114.6%. When the thickness of the water and mud resistant rock mass is 4 m, although some blocks at the bottom of the water and mud resistant rock mass appear to be peeling and slipping, the vertical displacement of the water and mud resistant rock mass is relatively weakened from the perspective of the overall structure of the water and mud resistant rock mass. No matter how high the safety thickness is, each measuring point on the measuring section at the bottom of the water and mud-resistant rock mass has a high vertical displacement, and the damage degree at the dome is relatively serious.

3.3.2. Evolution Characteristics of Seepage Pressure under Different Thickness. Figure 16 shows the evolution process of the seepage field in the water and mud-resistant rock mass under the different safety thicknesses ($d = 2$ m, 3 m, and 4 m), the karst water pressure is 1 MPa, the tunnel depth is 500 m, and the inclination of the joint is 15°.

It can be seen from Figure 16 that in different thicknesses of the water and mud-resistant rock mass, the process of progressive seepage failure in the entire water and mud-

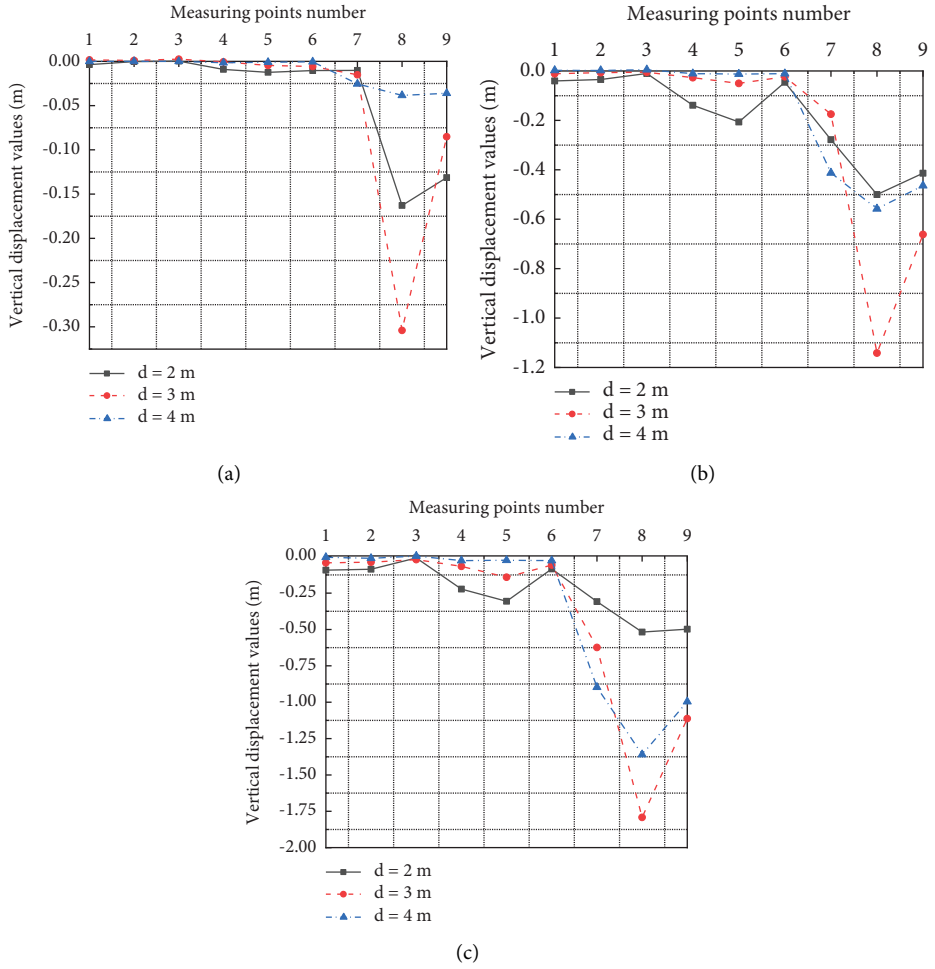

Figure 15: Evolution characteristics of displacement in the measuring points. (a) $t = 1$ s. (b) $t = 3$ s. (c) $t = 5$ s.

resistant rock mass is similar. That is to say, the combined effect of karst water pressure and blasting excavation disturbance causes the continuous initiation of fissures in the water and mud-resistant rock mass, and the effect of seepage erosion is gradually prominent, and the seepage path is continuously adjusted with the initiation of cracks. The expansion and penetration of the cracks in the water and mud-resistant rock mass will eventually lead to the failure of seepage instability. Through the comparative analysis of the numerical results in Figure 16, it can be seen that the different thicknesses of the water and mud-resistant rock mass have a significant effect on the seepage pressure and seepage area of karst water. When the thickness of the water and mud resistant rock mass is 2 m, the fracture and fragmentation degree of the entire water and mud resistant rock mass and the influence range of the seepage area are more extensive than those when the thickness is 3 m and 4 m. The numerical calculation results show that the smaller the thickness of the water and mud-resistant rock mass in the karst tunnel, the weaker the stability of the water and mud-resistant rock mass structure under the influence of external factors, the more serious the degree of rupture and fracture, the wider the influence of the seepage area, and the more likely the tunnel will occur.

Figure 17 shows the evolution process of the seepage pressure at different measuring points in different thicknesses of the water and mud-resistant rock mass. Regardless of the thickness of the water and mud-resistant rock mass, the fissure water in the water and mud-resistant rock mass can always penetrate to the $n_1 \sim n_3$ measuring points under the action of karst water pressure, and the seepage pressure value is stable at about 1 MPa. When the thickness of the water and mud-resistant rock mass is 2 m, the seepage pressure values of measuring points are significantly higher than those of other thicknesses. This is because when the thickness is 2 m, with the increase in calculation time, the rock mass structure in the water and mud-resistant rock mass is cracked under the action of karst water pressure, and the karst water gradually seeps and migrates along the crack channel. At $t = 5$ s, the karst water has covered the entire water and mud-resistant rock mass, and the karst water inrush channel is completely connected. Therefore, the water pressure value of each measuring point is relatively high when the thickness of the water and mud-resistant rock mass is 2 m. When the thickness is 3 m or 4 m, due to the increase in the safety thickness of the water and mud-resistant rock mass, the stability of the entire structure is significantly enhanced. During the numerical calculation process, the

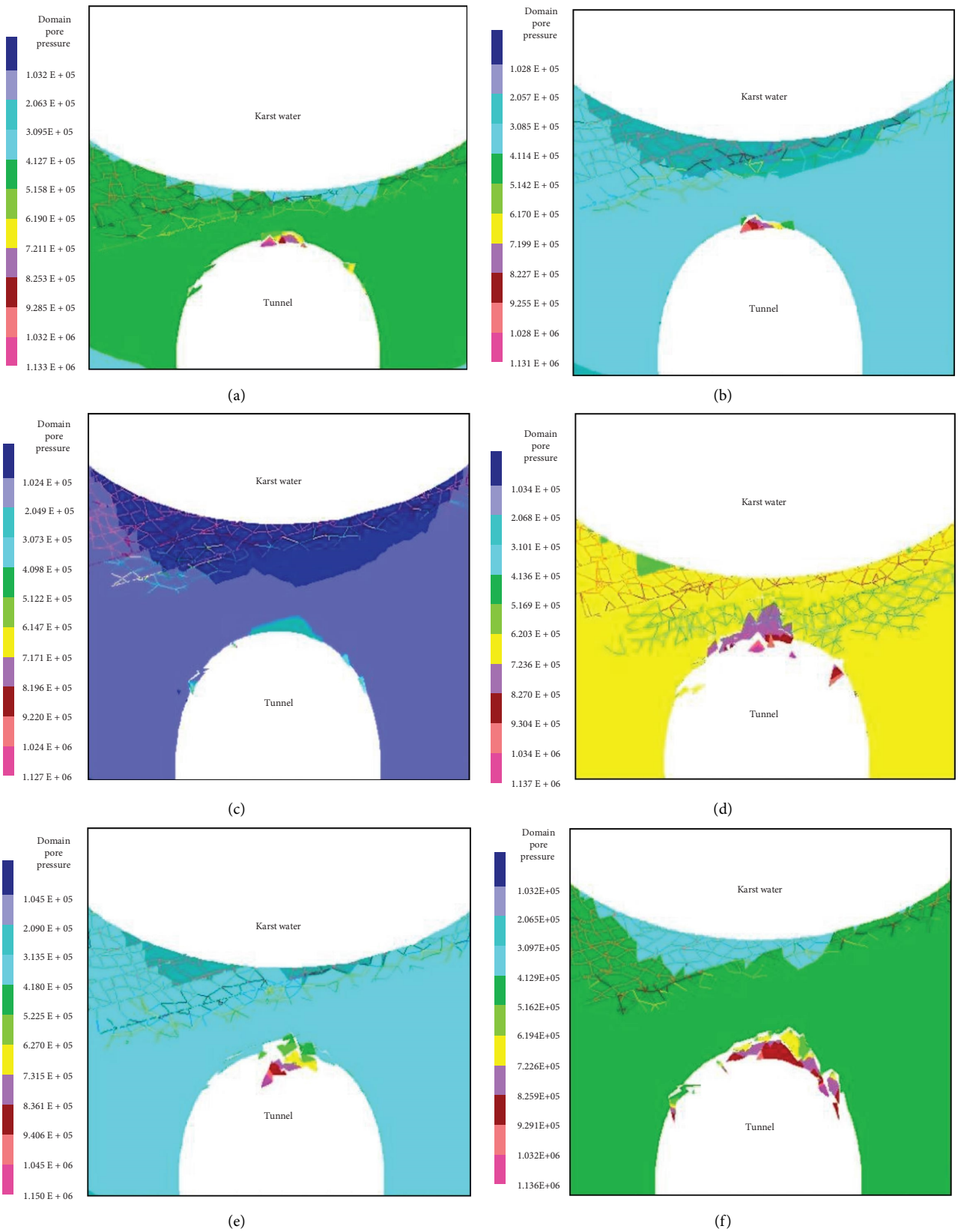

Figure 16: Continued.

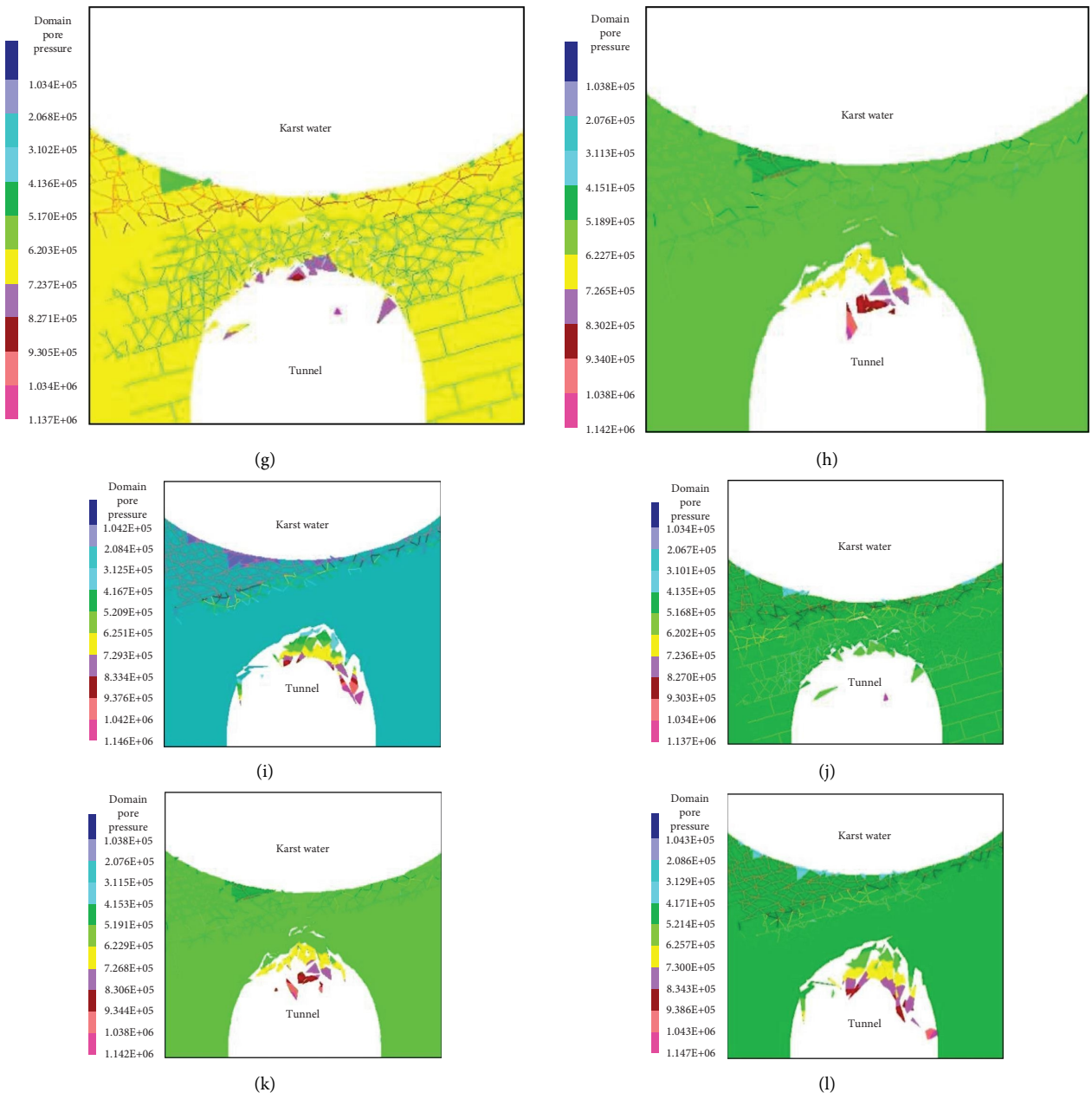

Figure 16: Evolution characteristics of seepage pressure under different thicknesses. (a) $t = 1$ s, $d = 2$ m. (b) $t = 1$ s, $d = 3$ m. (c) $t = 1$ s, $d = 4$ m. (d) $t = 3$ s, $d = 2$ m. (e) $t = 3$ s, $d = 3$ m. (f) $t = 3$ s, $d = 4$ m. (g) $t = 5$ s, $d = 2$ m. (h) $t = 5$ s, $d = 3$ m. (i) $t = 5$ s, $d = 4$ m. (j) $t = 7$ s, $d = 2$ m. (k) $t = 7$ s, $d = 3$ m. (l) $t = 7$ s, $d = 4$ m.

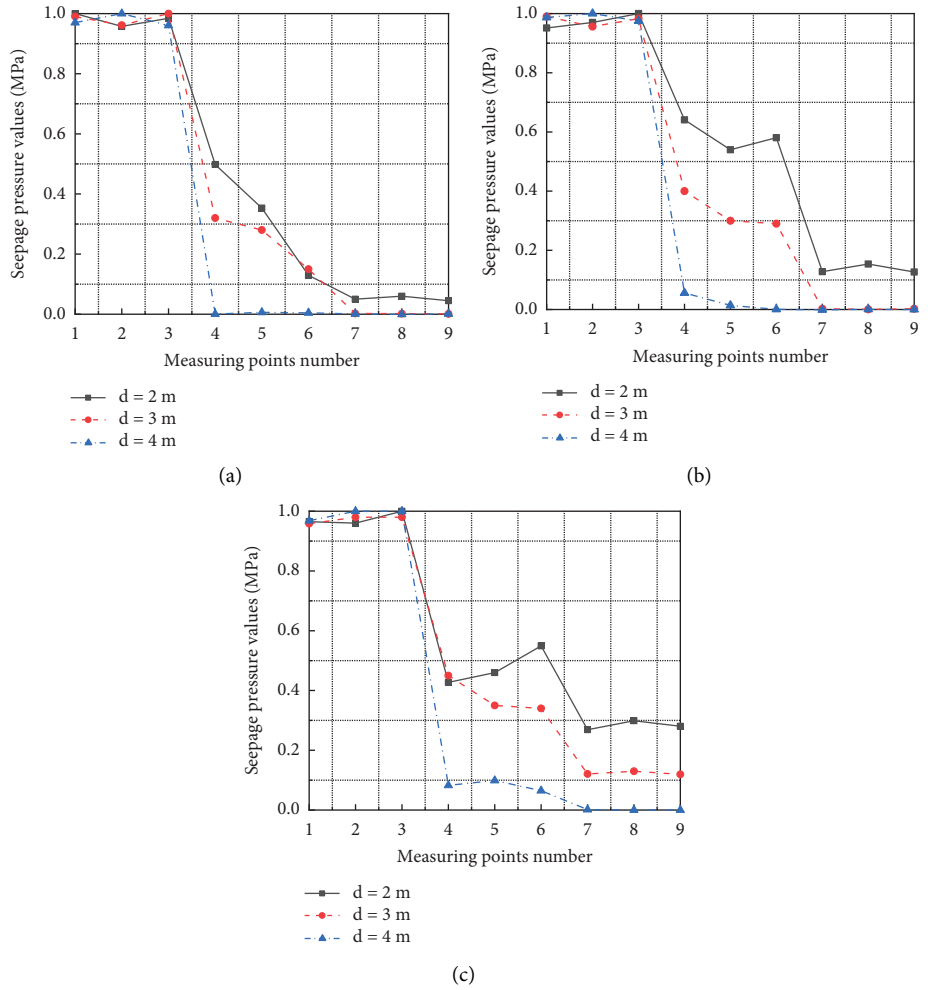

Figure 17: Evolution characteristics of seepage pressure in the measuring points. (a) $t = 1$ s. (b) $t = 3$ s. (c) $t = 5$ s.

water inrush channel is not completely formed, the water and mud resistant rock masses are relatively complete, and the water inrush resistance is stronger.

4. Conclusions

To investigate the evolution characteristics of catastrophe information in the water inrush under different conditions of joint dip angle, tunnel depth, and thickness of water and mud-resistant rock mass, a series of numerical simulation analyses based on DEM were conducted. Some conclusions can be drawn from the following:

(1) As the inclination angle of the joint increases, the vertical displacement value of each measuring point increases significantly, and the fracture area, fracture degree, and seepage pressure of the aquifer also increase rapidly. The seepage pressure of measuring points in the water and mud-resistant rock mass increases with the increase in the inclination angle of the joint. The seepage pressure values of different measuring points showed a decreasing trend from HL_1 to HL_3.

(2) The area and magnitude of the water and mud-resistant rock mass displacement decrease with increasing tunnel depth. The seepage velocity and fracture propagation velocity of karst water vary greatly with the tunnel burial depth. As the depth of the tunnel increases, the distribution area of water cracks and hydraulic cracks decreases significantly, and water inrush is less likely to occur.

(3) With the increase of the water and mud-resistant rock mass thickness, the failure mode of the tunnel outburst layer structure gradually changes from the overall collapse to the partial collapse of the vault to form a relatively stable slump arch. The greater the thickness of the water and mud-resistant rock mass, the higher the critical water pressure for failure and instability, and the stronger the antioutburst ability.

Data Availability

The data used to support the findings of this study are available from the corresponding author upon request.

Conflicts of Interest

The authors declare that they have no conflicts of interest.

Acknowledgments

This research was financially supported by the National Natural Science Foundation of China (Grant no. 52178388), the National Key Basic Research and Development Plan (973 Plan) Project (Grant no. 2013CB036003), the China Postdoctoral Science Foundation Fund (Grant no. 2018M631114), and the Key Scientific and Technological Project of Henan Province, China (Grant no. 212102310292).

References

[1] S. C. Li, J. Wu, Z. H. Xu, L. Zhou, and B. Zhang, "A possible prediction method to determine the top concealed karst cave based on displacement monitoring during tunnel construction," *Bulletin of Engineering Geology and the Environment*, vol. 78, no. 1, pp. 341–355, 2017.

[2] W. L. Wu, X. L. Liu, J. Q. Guo, F. Y. Sun, X. Huang, and Z. G. Zhu, "Upper limit analysis of stability of the water-resistant rock mass of a karst tunnel face considering the seepage force," *Bulletin of Engineering Geology and the Environment*, vol. 80, pp. 5813–5830, 2021.

[3] H. R. Zarei, A. Uromeihy, and M. Sharifzadeh, "Evaluation of high local groundwater inflow to a rock tunnel by characterization of geological features," *Tunnelling and Underground Space Technology*, vol. 26, no. 2, pp. 364–373, 2011.

[4] F. Gutiérrez, M. Parise, J. De Waele, and H. Jourde, "A review on natural and human-induced geohazards and impacts in karst," *Earth-Science Reviews*, vol. 138, pp. 61–88, 2014.

[5] Y. X. Lv, Y. J. Jiang, W. Hu, M. Cao, and Y. Mao, "A review of the effects of tunnel excavation on the hydrology, ecology, and environment in karst areas: current status, challenges, and perspectives," *Journal of Hydrology*, vol. 586, Article ID 124891, 2020.

[6] S. C. Li, Z. Q. Zhou, L. P. Li, Z. H. Xu, Q. Q. Zhang, and S. S Shi, "Risk assessment of water inrush in karst tunnels based on attribute synthetic evaluation system," *Tunneling and Underground Space Technology incorporating Trenchless Technology Research*, vol. 38, pp. 50–58, 2013.

[7] P. Jeannin, A. Yves, and D. Malard, "Assessing karst-hydraulic hazards in tunneling-the Brunnmühle spring system-Bernese Jura, Switzerland," *Environmental Earth Sciences*vol. 74, pp. 7655–7670, 2015.

[8] Y. G. Xue, F. M. Kong, D. H. Qiu, M. Su, Y. Zhao, and K. Zhang, "The classifications of water and mud/rock inrush hazard: a review and update," *Bulletin of Engineering Geology and the Environment*, vol. 80, no. 3, pp. 1907–1925, 2021.

[9] X. X. Liu, S. L. Shen, Y. S. Xu, and Z. Y. Yin, "Analytical approach for time-dependent groundwater inflow into shield tunnel face in confined aquifer," *International Journal for Numerical and Analytical Methods in Geomechanics*, vol. 42, no. 4, pp. 655–673, 2018.

[10] Y. J. Zhao, F. G. Wang, C. S. Li, Y. Q. Cao, H. L. Tian, and L. Borrelli, "Study of the corrosion characteristics of tunnel fissures in a karst area in southwest China," *Geofluids*, vol. 2018, pp. 1–19, Article ID 6234932, 2018.

[11] Z. Huang, W. Zeng, Y. Wu, S. J. Li, and K. Zhao, "Experimental investigation of fracture propagation and inrush characteristics in tunnel construction," *Natural Hazards*, vol. 97, no. 1, pp. 193–210, 2019.

[12] M. Q. Zhang, H. J. Huang, S. X. Zhang, J. Wu, and X. H. Li, "Treatment technology for water and mud bursting on 1.21 in Maluqing tunnel of Yichang-Wanzhou railway," *Journal of Railway Engineering Society*, vol. 11, pp. 49–56, 2008.

[13] C. H. Bai, *Research on Intelligent Prediction Method of Hazard Risk of Water and Mud Inrush in Karst Tunnel Based on Machine Learning*, Shandong University, Jinan, China, 2021.

[14] S. C. Li, Y. C. Yuan, L. P. Li, Z. H. Ye, Q. Q. Zhang, and T. Lei, "Water inrush mechanism and minimum safe thickness of rock wall of karst tunnel face under blast excavation," *Chinese Journal of Geotechnical Engineering*, vol. 37, pp. 313–320, 2015, (in Chinese).

[15] Z. H. Xu, J. Wu, S. C. Li, B. Zhang, and X. Huang, "Semi analytical solution to determine minimum safety thickness of rock resisting water inrush from filling-type karst caves," *International Journal of Geomechanics*, vol. 18, no. 2, pp. 1–11, 2018.

[16] F. Huang, L. H. Zhao, T. H. Ling, and X. L. Yang, "Rock mass collapse mechanism of concealed karst cave beneath deep tunnel," *International Journal Of Rock Mechanics And Mining Sciences*, vol. 91, pp. 133–138, 2017.

[17] J. Q. Guo, J. X. Chen, F. Chen, S. X. Huang, and H. Y. Wang, "Using the schwarz alternating method to identify critical water-resistant thickness between tunnel and concealed cavity," *Advances in Civil Engineering*, vol. 2018, pp. 1–14, Article ID 8401482, 2018.

[18] L. Li, X. L. Rong, M. Y. Wang, H. Lu, and Y. P. Xia, "Development and application of 3d model test system for water inrush geohazards in long and deep tunnels," *Chinese Journal of Rock Mechanics and Engineering*, vol. 35, pp. 491–497, 2016, (in Chinese).

[19] A. Kirsch, "Experimental investigation of the face stability of shallow tunnels in sand," *Acta Geotechnica*, vol. 5, no. 1, pp. 43–62, 2010.

[20] G. Idinger, P. Aklik, W. Wu, and R. I. Borja, "Centrifuge model test on the face stability of shallow tunnel," *Acta Geotechnica*, vol. 6, no. 2, pp. 105–117, 2011.

[21] Z. Huang, S. J. Li, K. Zhao, Y. Wu, and Z. Wu, "Liquid-solid coupling model test to investigate seepage failure mechanism of intact confining rocks of tunnels," *Journal of Basic Science and Engineering*, vol. 27, pp. 1345–1356, 2019.

[22] Z. W. Liu, M. C. He, and S. R. Wang, "Study on karst water burst mechanism and prevention countermeasures in Yuanliangshan tunnel," *Rock and Soil Mechanics*, vol. 27, pp. 228–232, 2006.

[23] M. J. Zhao, X. H. Liu, J. H. Ao, and B. Wang, "Numerical analysis of influence of karst caves in top of tunnel on stability of surrounding rock masses," *Rock and Soil Mechanics*, vol. 24, pp. 445–449, 2003.

[24] L. Qin, L. Wei, J. X. Chen, Y. B. Luo, P. Huang, and Y. Y. Wang, "Stability analysis of water and mud resistant rock mass in karst tunnel based on releasable elastic strain energy," *Mathematical Problems in Engineering*, vol. 2017, pp. 1–9, 2017.

[25] T. Lei, M. S. thesis, *Mechanism and Safety Thickness Prediction of Water Inrush for Overlying Water-Filling Karst Cave in Tunnels and Engineering Applications*, M.S. Thesis, Shandong University, Jinan China, 2015.

[26] U. D. E. C. Itasca, *Manual: Universal Distinct Element Code Version 5.0*, Itasca Consulting Group Inc, Minneapolis, Minnesota, 2011.

[27] E. Eker and S. Akin, "Lattice Boltzmann simulation of fluid flow in synthetic fractures," *Transport in Porous Media*, vol. 65, no. 3, pp. 363–384, 2006.
[28] Itasca Consulting Group, *Inc. UDEC (Universal Distinct Element Code) User's Manual*, Itasca Consulting Group. Inc, Minnesota, 1996.
[29] T. X. Liu, *Mechanism Analysis and Model Test of Karst Roof and Pile Foundation*, Ph.D. Thesis, Central South University, Changsha, China, 2003.
[30] W. X. Zhu, *Study on Mechanism of Water Inrush in Muddy Limestone Karst Tunnel after Wetting and Drying Cycles*, Ph.D. Thesis, China University of Mining and Technology, Beijing, China, 2018.
[31] S. G. Chen and J. Zhao, "A study of UDEC modelling for blast wave propagation in jointed rock masses," *International Journal of Rock Mechanics and Mining Sciences*, vol. 35, no. 1, pp. 93–99, 1998.
[32] Z. Y. He, *Study on Progressive Failure and Safety Thickness of Water and Mud Inrush Resistant Rock Mass during Karst Tunnel Constructed by Drilling and Blasting Method*, M. S. Thesis, Henan Polytechnic University, Jiaozuo, China, 2017.
[33] L. P. Li, *Study on Catastrophe Evolution Mechanism of Karst Water Inrush and its Engineering Application of High Risk Karst Tunnel*, Ph.D. Thesis, Shandong University, Jinan, China, 2009.
[34] W. X. Zhu, H. W. Jing, L. J. Yang, B. Pan, and H. J. Su, "Strength and deformation behaviors of bedded rock mass under bolt reinforcement," *International Journal of Mining Science and Technology*, vol. 28, no. 4, pp. 593–599, 2018.
[35] C. W. Boon, "Study of reinforcement support mechanisms for wide-span horseshoe-shaped openings in horizontally layered jointed rock using the distinct element method," *Rock Mechanics and Rock Engineering*, vol. 52, no. 4, pp. 1179–1191, 2019.